SEARCH FOR COLLECTIVE PHENOMENA IN RELATIVISTIC NUCLEAR COLLISIONS

H. H. Gutbrod

Gesellschaft für Schwerionenforschung
Darmstadt, West Germany
and
Lawrence Berkeley Laboratory
University of California
Berkeley, CA 94720

I. INTRODUCTION

Relativistic nuclear collisions are very often expected to enable in an earthly laboratory the study of conditions of matter as they might exist in neutron stars. There, the astrophysicists lack the knowledge of star properties when densities of several times of nuclear density come into play. This nice link of relativistic nuclear physics to the Universe may be comforting. For relativistic nuclear collisions to fulfill these expectations they must yield information on the equation of state of nuclear matter of which very little is known.

Nuclei are finite pieces of nuclear matter and one of the first tasks is to find out how heavy nuclei have to be to show nuclear matter phenomena in their relativistic collisions. Are nuclei of Ne good nuclear matter probes or is it necessary to collide U with U for observing nuclear matter phenomena?

In Figure 1 the equation of state of nuclear matter is plotted in all its various forms of speculations. The experimentalist doing nuclear collision studies and detecting nuclear fragments at the time long past the primary stage is faced with the fact that in all reactions the available kinetic energy is transformed into heat, particle production, and perhaps also compression energy. It is necessary to find observables directly related to the extreme state of the early part of the reaction and to avoid a dilution of the content of information due to the later final state interactions. Another problem is the separation of single nucleon-nucleon collisions from multicollision or even collective phenomena. This is necessary before talking about matter properties. Thus the extraction of

the equation of state the main goal of studying relativistic nuclear collisionsis not an easy task .

Complementing the report of L. Schroeder, this report will focus on to the target rapidity and somewhat further on to the midrapidity region. Especially heavy targets and heavy beams will be subject of discussion in order to come as close as possible to nuclear matter studies. A more macroscopic viewpoint is taken with terms like bulkmotion, particle flux, energy flux, temperature, chemical equilibrium, etc. Not all of these terms are justified and some are highly disputable. A theoretical discussion along those critical points is done by M. Gyulassy in these proceedings.

In Figure 2 the schematic picture of the fireball model is shown. This model, developed by our collaboration[1]) several years ago and refined into the fire streak model,[2]) treats the reaction under the extreme aspect of total thermalization. The model is going through a "renaissance" since theorists find it practical to study all kinds of aspects (like Coulomb effects,[3]) Blast wave[4]) . . .). It is until now the only model which includes full particle production and cluster formation.

This report will show the weakness of the fireball/fire streak model[2]) and try to convince that more complex models are necessary and even available to close in on the data. It will first discuss the single particle spectra of nucleons, clusters and pions, then focus onto the fate of the target nucleus, look onto possible evidence of collective phenomena and finally discuss the data which are selecting on central collisions and reflecting the nature of the energy flux in the target nucleus.

II. SINGLE PARTICLE INCLUSIVE DATA

Lee Schroeders report in these proceedings points out the various features of high energy proton spectra from relativistic nuclear collisions taken mainly by S. Nagamija and collaborators.[5]) There it is shown that the momentum distribution goes to more than twice the beam value.

In a clean knock out model--comparable to the first collision in a full cascade model--Hatch and Koonin[6]) show that the Fermi motion has to be included to explain the data.

A total different view point is taken when looking at the thermal picture. Many collisions (more than 2) are necessary to justify it. The agreement of data and calculations with the fire streak[2]) (including chemical equilibrium) showed slightly better agreement with these data than the clean knock out model with Fermi motion.

Protons

A more detailed comparison with data is necessary to find out whether the simple thermal model really describes the inclusive data. Therefore, the region of maximum cross section has been chosen which is between 20 and 200 MeV. Figure 3 shows proton spectra from the reaction of Ne on U at four different energies.[7]) There is a obvious strong disagreement with the data at 30° for all energies and a fair agreement at low energies and large angles which disappear at high energies. Objections are voiced against the present fire steak calculations in as they neglect the Coulomb force.[8]) Coulomb effects are expected to be significant for low proton energies and heavy nucleus systems. Therefore looking into the Z_{target} dependence the fire streak model[2]) is compared with data from 400 MeV/u Ne interactions with targets from U to Al.[7]) Especially the light target of Al should be an example where Coulomb effects are negligible and the present fire steak model might work as is. Figure 4 shows proton spectra from Ne + U, Ne + Au, Ne + Ag, Ne + Al at 400 MeV/u. The fire streak calculations are fairly good at backangles (ignoring a factor of 1.5 to 2), however for all targets the forward angle is totally off.

Thus, the thermal model with its clean-cut, no deflection geometry, cannot describe the data and the model cannot be made to fit by introducing the proper treatment for the Coulomb force.

Neutrons

When data disagree with ones expectation, those data are exciting and surprising. In 1979 the measurement of single neutron inclusive data[9]) showed a surprising difference to the single proton inclusive data. For a uranium target the neutron/proton ratio exceeded by far the value of 1.6 expected

from the neutron excess in the target nucleus. Later neutron data from ^{20}Ne on ^{27}Al (Ref. 10) did not show a large discrepancy to the existing proton data. Again, the discrepancy of uranium was tried to be explained by the effect of the Coulomb force onto the protons which supposedly changes their spectrum.[8])

However, recently Stevenson[11]) and independently Stock[12]) came up with a straight forward explanation based on the experimentally observed large cluster production in relativistic nuclear collisions.[7]) Figure 5 points out for Ne + U reactions the small percentage of free protons emitted (~30 percent) versus the large amount of bound protons emitted in clusters (up to 60 percent). Since the clusters are dominantly T = 0 fragments--the yield of tritons is similar to that of ^{3}He--the large n/p ratio for reactions on uranium can be easily understood: Due to the removal of on-the-average T = 0 fragments a system with a neutron excess to begin with will end--in the extreme situation--in a pure neutron system. Stevenson[11]) shows in Figure 6 that there is no anomalous neutron/proton ratio if all neutrons and protons bond in the emitted clusters are also counted properly. This successful explanation of the neutron/proton ratio leads directly back to the previous subject of how to describe consistently the single proton data and how to treat the cluster formation.

Summed Charges

The description of the nucleon emission with respect to the single particle inclusive data is well under way by several groups some of which take the intra-nuclear cascade--some the hydrodynamical picture as basis for this model. A detailed report has been given by M. Gyulassy and C. Schroeder in this serie. Figure 6 shows results from the cascade calculation by Stevenson[11]) from Berkeley. Figure 7 has on the left side the calculations (histograms) of the cascade code of Fraenkel and Yariv[15]) from Rehovot, on the right side is a comparison of the summed-change data with two-fluid hydrodynamics calculations.[16]) These models do not yet treat the cluster emission and are compared therefore with pseudo-proton spectra (summed charges), where the proton-, deuteron-, triton- and twice the ^{3}He- and ^{4}He-double differential cross sections have been added up for given MeV/u bins to

produce somehow a spectrum close to the primary proton distribution. This binning in Mev/u is, however, only allowed if mean field effects are not different for protons or neutrons. If the reaction is dominated for a certain fragment energy by the Coulomb force, as S. Koonin and others claim, then such a simple summing in charges is only valid way above the Coulomb peak of fragment spectra or where Coulomb effects can be neglected. These summed charges of various reactions are fairly well described over all incident energies from 250 to 2100 MeV/u by both the cascade and the hydrodynamical calculations. The complexity of these calculations unfortunately has not yet allowed to investigate thoroughly with statistical significance any deviations and their dependence with various quantities or parameters, e.g., different assumptions on the equation of state. Thus, there is the unusual picture of histograms presenting theory and smooth lines presenting data. It is remarkable, however, to see the cascade--and the hydrodynamical model to agree within a factor of 2 despite the totally different ansatz of each one. There are trends visible indicating that there are differences. The hydrodynamical code needs to produce a "transparancy" to describe the forward flux. This may be a point that the treatment of both nuclei as a fluid is exaggeration. One should keep in mind that there is a vapor layer on each fluid surface. Thus, the hydrodynamical behavior might be found only in part of the reaction zone. A restriction of data to small impact parameter collisions, if experimentally possible, would not totally avoid having surface spots which should be more appropriately treated as a nucleonic gas.

Clusterproduction

The clusterproduction has been approached in various ways, e.g., via a coalescence model[14]) or in a chemical equilibrium model.[13]) The various ways and their different view points are well described by J. Kapusta (ref. 13):

The coalescence model assumes that two nucleons close together in momentum space can coalesce if they can give off excess energy and momentum to a third body, be it a simple particle or an optical potential of a large nucleus.

If $\gamma d^3n_N/dp^3$ is the relativistically invariant momentum space density for nucleons before the coalescence process then the probability for finding one nucleon inside a sphere with radius p_o at momentum p

$$P(1) = \frac{1}{M} \frac{4\pi}{3} p_o^3 \left(\gamma \frac{d^3n_N}{dp^3} \right)$$

where M is the mean nuclear multiplicity. Purely statistically, two nucleons are found in that sphere with the probability:

$$P_M(2) = \binom{M}{2} P^2(1)(1 - P(1))^{M-2}$$

If $M<<1$ and $MP<<1$ then $(1 - P(1))^{M-2}$ is approximately one.

$$\gamma \frac{d^3n_{deuteron}}{dp^3} = \frac{1}{2} \frac{4\pi}{3} p_o^3 \left(\gamma \frac{d^3n_N}{dp^3} \right)^2$$

No distinction is made between neutron- and proton-distribution nor has the spin been taken care of. The main finding is that the deuteron cross section is proportional to the square of the proton cross section. For heavier clusters like an α-particle its cross section would be the fourth power of the proton cross section, etc.

The thermal model assumes an emitting system with both kinetic and chemical equilibrium. Given the baryon number, energy, charge and density of the emitting system then the volume V, temperature τ and neutron and proton chemical density μ_n and μ_p can be calculated.

The distribution of particles of type i in momentum space is

$$\frac{d^3n_i}{dp^3} = \frac{2S_i + 1}{(2\pi)^3} V \left[\exp \frac{(p^2 + m_i^2)^{1/2} - \mu_i}{T} \pm 1 \right]^{-1}$$

Where S_i is the spin and refers to fermious or bosons. Assuming non-degenerate particles in low density the deuteron cross section is in terms of Lorentz invariant densities

$$\gamma \frac{d^3 n_{deuteron}}{dp^3} = \frac{3}{4} 8 \frac{(2\pi)^3}{V} \frac{1}{\gamma} \left(\gamma \frac{d^3 n_{proton}}{dp^3}\right)\left(\gamma \frac{d^3 n_{neutron}}{dp^3}\right)$$

Kapusta compares 2 more clusterformation models, but all of them have the power law dependance between cluster and single particle cross sections. Figure 8 shows some old data[1]) of high energy Boron emitted from the reaction of 343 MeV/u ^{20}Ne with U and a thermal fit to the spectrum. The velocity and the temperature is very close to the values for a compound nucleus-system.

Whereas the physical significance of the coalescence model is not easy to grasp--the physics is covered up in the value of p_o--the thermal model allows to calculate the cluster-production based on a freeze out volume or rather freeze out density. However, the clusterproduction up to now has been only studied for single particle inclusive cross setion ignoring the possibility that there are events with predominantly cluster emission versus events with predominantly nucleon emission. It is interesting to see in future experiments whether we find some information on the entropy of in the early system via the measurement of cluster to nucleon ratios the events. The problem of clusterformation will be discussed later on again for heavier fragments. Data on cluster emission are plentiful available and more effort is definitively needed on the theoretical side.

Pions

Whereas the emitted protons come from the projectile and/or target nucleus, under-going one or many collisions, the emitted pions are created in the collision and thus carry hopefully the information about the early stage of the reaction. The low energy pions are expected to be least affected by absorption equivalent to a large mean free path as long as their energy is below that of the $\Delta(1232)$ resonance energy. Out of many samples of pion data[18]) the pion production in the reaction of 1.05 GeV/n ^{40}Ar or ^{40}Ca is chosen[19])

since it has stirred quite some interest. Figure 9 shows the contours of constant invariant cross sections for pions produced in the reaction of 1.05 GeV/u ^{40}Ar or ^{40}Ca[19]) and of 730 MeV protons on hydrogen.[20]) The proton data can be understood in terms of the decay of an isobar nearly at rest in the center of mass producing a characteristic forward-backward peaking. In contrast to that there is a peak in the midrapidity region for ^{40}Ar + ^{40}Ca.

Koonin et al.[3]) try to describe the observed phenomenon with the help of "Coulomb focusing." The two nuclei pass each other, the interaction-region forms a fireball and, after the passage time of more than 10^{-22} sec, the emitted pions see the Coulomb fields of the outgoing two remnants besides that of the fireball and are focussed into 90° C.M. Figure 10 shows, besides the data in the upper left comer, the calculations assuming different fractions of the fireball charge as calculated in the fireball geometry. In the lower right side of Figure 10 the authors[3]) calculated a contour diagram for pion production from a near central collision of ^{40}Ar or ^{40}Ca. Despite this encouraging agreement the authors point out that a much more complicated pion emission pattern is necessary to fullfill certain aspects of the data. Their exciting conclusion is that "some charge must remain nearly at rest in the center of mass after the collision probably dispercing on a time scale of 10^{-22} sec." These data however have been studied in more detail than just single particle inclusive. When only those events were looked at where a total disintegration of the target and projectile nuclei occurred--thus, no big spectator charge was left to focus--then the π^+ enhancement still remainder. Besides such a fascinating aspect of having a glimpse of the NUFO[21]) there is another explanation of this midrapidity peak at least as fascinating: Greiner et al.[22]) predicted a collective hydrodynamic flow which could also account for the preferential sidewise ejection of pions observed here. Further calculations are necessary to clear these phenomena and similar data of π^- emission in this system 1.05 GeV/u ^{40}Ar + ^{40}Ca are needed to clarify the importance of Coulomb effects, even for hydrodynamical models. Preliminary data by Sandoval et al.,[26]) indicate that the negative pions do not

simply follow the Coulomb recipe but some sidewise emittance remains. The bulk of π^+ data [18]) shows many more bumps which will require a lot of intuition and work until they are fully understood.

III. THE FATE OF THE TARGET NUCLEUS

The energy dissipation in large targetnuclei like U and Au is the dominant theme of the following studies. At first nucleon-nucleon-collision was considered to be the basic determining process in the relativistic nuclear collisions thus the E/u of the projectile was expected to be a reasonable guideline in the comparison of reactions with different projectiles. It was a big surprise when in the various experiments more and more the total kinetic energy of the projectile became the important quantity rather than the velocity and the size of the projectile independently. In this chapter, data of very slow fragments and their correlation to the fast particles, previously discussed, are looked at to tell of the late state of the reaction process. For a better understanding of the data, first a tour will be given through the experimental details.

a) Experimental Apparatus

The apparatus used, which is schematically shown in Fig. 11, consisted of three distinctive different types of equipment; (1) particle telescope, (2) silicon array, (3) plastic scintillator array. The particle telescope and silicon array were each mounted on independently moveable arms inside the one meter diameter scattering chamber. The plastic scintillator array was mounted in air outside the walls of the chamber.

The particle telescope consisted of a ΔE gas ionization chamber and three silicon surface barrier E detectors. The ionization chamber was a large volume (14.8 x 9.8 x 5.3 cm) Frisch grid chamber with an active cathode repeller plate. The chamber had a 50 $\mu g/cm^2$ polypropylene entrance window and was operated with methane gas at a pressure of 20 Torr. The three 6 cm^2 active area, 100 μm thick E detectors each

had an angular resolution of 2^{o} and their centers were separated by an angle of 5.5^{o}. The telescope, which subtended a solid angle of 11.5 msr, was calibrated with ^{241}Am and ^{148}Ge alpha sources as well as with a ^{252}Cf spontaneous fission source. It was sensitive to particles with $Z \geq 4$ and energies larger than 5 MeV and less than 150 MeV.

The silicon array consisted of five 6 cm^2 active area, 100 μm thick silicon surface barrier detectors and was sensitive to any particle depositing 6 MeV or more. Three of the detectors were oriented in the reaction plane as defined by the target, telescope, and beam. Each detector had an angular acceptance of 5^{o} and their centers were separated by an angle of 15^{o}. The array subtended a solid angle of 127.2 msr and was calibrated with ^{241}Am and ^{148}Gd sources as well as with a ^{252}Cf spontaneous fission source.

The plastic scintillator array consisted of 80 plastic scintillators 1/4 inch thick which were coupled to photomultiplier tubes by means of lucite light pipes. Seventy-six of the scintillators were arranged in three azimuthal rings (A, B, and C) which subtended theta angles of 9^{o} to 20^{o}, 20^{o} to 45^{o}, and 45^{o} to 80^{o}, and accounted for 67% of the forward 2π. The remaining four scintillators (Ring D) were oriented in the reaction plane and subtended theta angles of 120^{o} to 160^{o} on both sides of the beam axis.

A monitor telescope was used for relative normalization of each run.

The associated charged particle multiplicity information was obtained by measuring the number of fast charged particles that triggered the scintillator array in coincidence with observing a particular fragment in the particle telescope. The low energy threshold for observing particular charged particles in the plastic scintillators is equivalent of 25 MeV protons. One quantitative piece of information that can be extracted from these measurements is the average real associated charge particle multiplicity. This average multiplicity was determined by adopting the standard techniques developed for γ-ray multiplicity measurements correcting for missing solid angle, coincidence summing, and accidental and dead time probabilities, assuming uniform azimuthal distributions and no correlations in particle emission. This procedure was applied

to the multiplicity information in each of the four rings yielding a quantity $d\langle m\rangle/d\Omega(\theta)$. The average real multiplicity was determined by integrating $d\langle m\rangle/d\Omega(\theta)$ from 0 to π. The accidental and deadtime probabilities were small, of the order of a few percent, in all cases.

The final piece of information obtained from this experiment concerns azimuthal correlations ($d^2\sigma/d\Omega_1 d\Omega_2(\phi)$, where $\phi = |\phi_1 - \phi_2|$) between slow fragments detected in the particle telescope and fast particles detected in the plastic scintillator array. In order to determine if such a correlation exists, a two particle correlation function was extracted from the data. In particular, the R function which is defined as

$$R = \sigma_R \frac{\frac{d^2\sigma}{d\Omega_1 d\Omega_2}}{\frac{d\sigma_1 d\sigma_2}{d\Omega_1 d\Omega_2}} - 1$$

was used, where σ_R is the total inelastic cross-section and $d\sigma_1/d\Omega_1$ and $d\sigma_2/d\Omega_2$ are the single particle inclusive cross-sections for particle 1 and 2 respectively.

Figure 12 shows the charged particle multiplicity distribution associated with a proton of an energy of 40 to 200 MeV detected at 90° (Lab) when a U-target was bombarded with 42 GeV ^{40}Ar or 42 GeV ^{20}Ne, resulting in nearly identical distributions.[7]) Further investigation yielded the data in Figure 13. The average total charged particle multiplicity associated with a proton, or deuteron or triton detected at 90° (Lab) rises smoothly and, within a few units, the multiplicity is independent of projectile.[7,27]) The multiplicities are somewhat larger when associated with a deuteron or triton than with a proton. The next Figure 14 illustrates the same findings for the charged particle multiplicity associated with the emission of slow fragments of Z between 4 and $Z \geq 26$.[28]) It is shown that reactions of 8.4 GeV ^{4}He with Au--where the incident ^{4}He energy is way above the pion threshold--lead to the same destruction of the Au nucleus as do 8 GeV ^{20}Ne--with the incident Ne energy just above the pion threshold. It is also shown that at half the energy of the incident ^{4}He, the associated charged particle multiplicity is much lower. These slow fragments are

also characterized by the absence of zero multiplicities indicating that they come almost exclusively from central collisions.

This findings suggest that e.g., a 2.1 GeV/u ^{4}He as well as the slower 400 MeV/u Ne projectile get stopped in the large target-nucleus in such a short distance that there is enough nuclear matter still available to dissipate the deposited energy over most of the target nucleus, independent of the lucident particle velocity. As shown in Fig. 8 the thermal model fit to the Boron data predicts a hot moving source with a temperature of 27 MeV and a $\beta = 0.06c$ equivalent to a total dissipation of the incident energy in the target nucleus. This picture is supported by both cascade calculations (Toneev,[29]) Smith[30]) and hydrodynamical calculations[16,31])) where in heavy targets the light projectiles are quickly stopped leading to high density region in the early stage of the reaction close to the impact zone, and followed by an expansion and heating process involving most of the target nucleus.

Attempts made by Yariv and Fraenkel[15]) to describe associated charged particle multiplicity distribution show at first sight a remarkable closeness to the data, in a second investigation, however, the cascade calculations have systematic deviations from the data. More calculations and comparisons with the data are needed to clear up the nature of the observed deviations.

As a side remark: The nearby total simulation of the experimental conditions by Yariv and Fraenkel[15]) and also Noack[17]) in their computer codes are a fantastic help to the experimentalist since it allows to stay as close as possible near the raw data, a plus which is greatly appreciated in multi-correlation experiments.

Correlations Between Fast and Slow Fragments

All the thermal models, so far, have not incorporated any transverse momentum transfer from the reaction zone into the spectator matter. Thus the observation of the "spectators" would yield definite information on such an energy and momentum flux from the early stage of the reaction.

The fragments measured in this experiment can provide this information because they are target fragments. Of interest is

whether there is any correlation in space in the multiplicity pattern with respect to the reaction plane defined by the target and the telescope.

Figure 15 shows the correlation function of fragments of various Z from the reaction of 400 MeV/u ^{20}Ne + Au (lower 3 portions) and of 400 MeV/n ^{20}Ne + U for Z > 26 fragments which were identified as being predominately fission products associated with a very low multiplicity.[28]) There is a clear 180° in-plane correlation visible for the two middle cases for fragments with $13 \leq Z \leq 26$ and Z > 26. A heavy fragment gets pushed out to e.g., 90° whereas many fast fragments are emitted into the opposite direction in ϕ. This finding is to be explained, with momentum conservation, of course, however, it clearly points towards the link between the fast and the slow fragments and the reaction-mechanism has to be understood. (A long range Coulomb-repulsion of a second large body like in a binary fission process can be ruled out). Such a bounce-off-effect has been pointed out earlier[34]) to be visible in the hydrodynamical model calculations[16]) and recently Stöcker et al.[31,35]) have done a thorough theoretical analysis (Figures 16) discussing the deflection of the projectile as a function of impact parameter. They point out that this bounce-off effect could be a good method of studying the equation of state since it is a measure of the pressure produced in the reaction zone, be it from compression or be it from the heat. There is more information in the spectra of the slow fragments.

Fragment Spectra

Since the light fragments are earmarked by a dominately high associated charged particle multiplicity they come from very violent reactions where large amounts of energy are dissipated in the target nucleus. Figure 17 shows the 90° spectra of fragments of Z = 6 to Z = 11 from 1.05 GeV/u ^{4}He + Au. As in high energy proton-nucleus reactions the peak energy shifts towards higher values with increasing atomic number. It is found that the peak energy decreases for higher energies simultaneously with the increase of the associated charged paticle multiplicity. Also the slope of the spectrum gets flatter suggesting an increase in

"temperature" of the emitting system if such a unique system would exist. Following the conventional two-step model the emitting system can be treated in first guess as consisting of less charges than the sum of $Z_{projectile} + Z_{target} - Z_{fragment} - \langle M \rangle$. The peak energy, associated with the Coulomb barrier of the "evaporating" system, reflects then a reduced Coulomb radius of $r_{oc} = 2.0$ fm for the systems studied. On one side the mystical factor of $k = 0.5$ used in the analysis of high energy proton nucleus reactions for the description of the Coulomb peak is more illuminated. On the other side, the large reduced Coulomb radius of 2 fm indicates that there is a huge deformation in the system. Therefore, it is suggested to drop the two-step model and to look out for a more consistent but not necessarily simpler explanation.

Figure 18 offers the suggestive picture of a central collision as painted by a proponent of the hydrodynamic model. There the shape of the target nucleus developes, after a central collision, into that of a bowl. It can even lead to the formation of doughnut nuclei as suggested by C. Y. Wong. Then, of course, the emission from such a system is polarized to the beam direction. Most probably, there is not an overall constant temperature and certainly is the Coulomb force varying with the polar angle of emission. If this picture is correct then there is no easy way to extract the parallel momentum (or forward velocity) of the emitting system. It should be comforting to remember that simple models are not always right!

High Multiplicity Selected Data

It has been shown that in reactions on heavy targets slow light fragment emission occurs only in violent reactions. The slow fragments might not give the whole picture since for higher and higher deposition energies a total target and projectile disintegration into pions and nucleons has been observed. Figure 19 shows such data[14]) collected with the streamer-chamber where at 1.8 GeV/u ^{40}Ar collides with KCl and total disintegration into protons and pions has been observed. Thus, another step over and above single particle

inclusive data is: to select and study spectra from events characterized by a high charged particle multiplicity, therefore by a high energy flux. In the common understanding this restricts the impact parameters to dominantly small ones, if the assumption holds that the multiplicity of an event increases with decreasing impact parameter. It may well be, by the way, that the multiplicity of charged particles does not change much between an absolute central collision and the last possible impact parameter which allows the projectile to dive fully into the large target nucleus. Such a selection does not totally rule out the contributions of single collisions in the spectra (they occur also in central collisions), but greatly enhances the probability for multicollision processes.

The Figure 20 shows proton spectra for high and low multiplicity events for various incident energies of ^{20}Ne on U.[27]) When in Figure 3 the 30° spectra did not change for incident energies, the high multiplicity selected spectra at 30° get flatter with increasing Ne energy. The low multiplicity selection shows however again the features of the unselected data (Figure 3). When the high multiplicity selected spectra are looked at for various targets (Figure 21),[27]) the stronger suppression of the forward angle in the heavier targets is pointed out. When plotted in form of contours of constant invariant cross section in a $p_\perp$ - y plane (Fig. 11) the contourlines are centered close to the target rapidity and move only slowly to larger rapidity values when lower cross sections are considered. A sudden and strong stopping of the projectile inside the target nucleus must have occurred in order to create such an emission pattern. A reversed picture is given in Fig. 23 when protons from 1.05 GeV ^{40}Ar on ^{40}Ca are selected for high or low multiplicity: The low multiplicity protons cluster around the target region and the high multiplicity protons favor the midrapidity region, coinciding with the center of mass of this system. It is also there where a nuclear fireball would be a rest. Going back to the ^{20}Ne on U reaction where the forward emission is suppressed, this effect is so strong that when looked at in the form of an angular distribution for fixed fragment momenta even a side

wise emission is indicated,[32]) (Figure 24 and 25). For low momentum deuterons this effect is strongest.[27]) The hydrodynamical calculations describe such a suppression and even a strong sidewise emission for very central collisions. The quality of agreement, however, is poor as discussed in M. Gyulassy's report.

CONCLUSION

This report followed through single particle conclusive data to more complex measurements of observables with an inherent collective character. The observation of cluster-emission and of the bounce-off effect as well as the emission pattern of pions and protons in high- or low multiplicity events represent a large amount of data waiting to be attacked by sophisticated theories. Several phenomena were shown indicating that the all dominating quantity in central relativistic nuclear collisions is the total kinetic energy pumped to the system. This requires a very fast dissipative process. The nuclear collisions are compared in their cluster-production mechanism with super novae explosions yet the interest in this mechanism has been damped so far, by simple but wrong phase space arguments of the coalescence model. There is hope that the cluster data carry much more physics than previously anticipated and more theoretical work focuses onto them. The equation of state was shown in Fig. 1 with all its speculative beauty. K. R. Gudima and K. D. Donnev[36]) are taking the existing data plus the theoretical speculation serious. In their ultra nuclear cascade calculation they define a density and a temperature. Since they describe with their model fairly well the data they do the next step: they look for the implications. Figure 27 shows the phase diagram for a transition into the pion condensate. The curves A and B are critical temperatures from Ref. 37(A) and 38(B). The dynamical phase trajectories are calculated for head-on collisions. Both theories A and B would say that above 500 MeV/u Ar + Ca the pion condensate is formed, for ca. 1×10^{-23} sec. It is?

ACKNOWLEDGMENTS

For the invitation to the Kikuchi-Summer School and to the Hakone-Seminar I am very grateful to Dr. Homma and to Dr. Nakai. I am very grateful to my colleagues wo made it possible through their enthusiastic collaboration in the last five years to collect all these data presented in this report. They are Drs. J. Gosset, C. H. King, G. King, Ch. Lukner, M. R. Maier, W. G. Meyer, Nguyen Van Sen, J. Peter, A. M. Poskanzer, H. G. Ritter, S. Sandoval, H. Stelzer, R. Stock, A. Warwick, F. Weik, G. Westfall, H. Weiman and K. Wolf. I appreciate many fruitful and clearifying discussions with Drs. M. Gyulassi and J. Knoll.

This work was supported by the Bundesministerium für Forschung und Technologie West Germany and by the Nuclear Science Division under contract No. W-7405-ENG-48 with the US. DOE.

REFERENCES

1) G. D. Westfall, J. Gosset, P. J. Johansen, A. M. Poskanzer, W. G. Meyer, H. H. Gutbrod, A. Sandoval, and R. Stock, Phys. Rev. Letters 37, 1202 (1976).
J. Gosset, H. H. Gutbrod, W. G. Meyer, A. M. Poskanzer, A. Sandoval, R. Stock, and G. D. Westfall, Phys. Rev. C16, 629 (1977).

2) W. D. Myers, Nucl. Phys. A296, 177 (1978).
J. Gosset, J. I. Kapusta, and G. D. Westfall, Phys. Rev. C18, 844 (1978).

3) K. G. Libbrecht and S. E. Koonin, Phys. Rev. Lett. 43, 1581 (1979) and M. Gyulassy and S. K. Kauffman, to be published.

4) P. J. Siemens and J. O. Rasmussen, Phys. Rev. Lett. 42, 880 (1979).

5) S. Nagamiya, I. Tanihata, S. Schnetzer, L. Anderson, W. Bruckner, O. Chamberlain, G. Schapiro, and H. Steiner, J. Phys. Soc. Japan 44, 378 (1978) and to be published.

6) R. L. Hatch and S. E. Koonin, Phys. Lett. 81B, 1 (1979).

7) A. Sandoval, H. H. Gutbrod, W. G. Meyer, A. M. Poskanzer, R. Stock, J. Gosset, J.-C. Jourdain, C. H. King, G. King, Ch. Lukner, Nguyen Van Sen, G. D. Westfall, and K. L. Wolf, preprint (1979) LBL-7766, submitted for publication.

8) M. Gyulassy and S. K. Kauffmann, February 1980, to be published.

9) W. Schimmerling, J. W. Kast, D. O. Dahl, R. Maidy, R. A. Cecil, B. O. Anderson, and H. R. Baldwin, Phys. Rev. Lett. 43, 1985 (1979).
10. W. Schimmerling, private communications.
11. J. D. Stevenson, Phys. Rev. Lett. 41, 1702 (1978) and private communications Jan. 1980, to be published.
12. R. Stock, private communications.
13. A. Mekjian, Phys. Rev. Lett. 38, 640 (1977); and Phys. Rev. C17, 1051 (1978); J. Kapusta, June 1979, LBL-9251, to be published.
14. H. H. Gutbrod, A. Sandoval, P. J. Johansen, A. M. Poskanzer, J. Gosset, W. G. Meyer, G. D. Westfall, and R. Stock, Phys. Rev. Lett. 37, 667 (1976).
15. Y. Yariv and Z. Fraenkel, Phys. Rev. C20, 2227 (1979).
16. A. A. Amsden, F. H . Harlow, and J. R. Nix, Phys. Rev. C15, 2059 (1977).
A. A. Amsden, A. S. Goldhaber, F. H. Harlow, and J. R. Nix, Phys. Rev. C17, 2080 (1978).
17. C. Noack, Code Simon 1980, Berkeley, January 1980.
18. K. S. Wolf, H. H. Gutbrod, W. G. Meyer, A. M. Poskanzer, A. Sandoval, R. Stock, J. Gosset, C. H. King, G. King, Nguyen Van Sen, and G. D. Westfall, to be published.
19. K. S. Wolf, H. H. Gutbrod, W. G. Meyer, A. M. Poskanzer, A. Sandoval, R. Stock, J. Gosset, C. H. King, G. King, Nguyen Van Sen, and G. D. Westfall, Phys. Rev. letters 42, 1448 (1979).
20. D. R. F. Cochran, P. N. Dean, P. A. M. Gram, E. A. Knapp, E. R. Martin, D. E. Nagle, P. B. Perkins, W. J. Shlaer, H. A. Thiessen, E. O. Theriot, Phys. Rev. D 6, 3085 (1972).
21. V. Manko, private communication, September 1979.
22. W. Scheid, H. Müller and W. Greiner, Phys. Rev. Lett. 32, 741 (1974).
23. W. Benenson, G. Bertsch, G. M. Crawley, E. Kashy, J. A. Nolen, Jr., M. Koike, M. Sasao, H. Bowman, J. G. Ingersoll, J. O. Rasmussen, and J. Sullivan, J. Peter, and T. E. Ward, Phys. Rev. Lett. 43, 683 (1979) and J. Rasmussen, private communications.
24. H. Stöcker, W. Greiner, W. Scheid, Z. Physik A 286, 121 (1978) and U. Heinz, H. Stöcker, W. Greiner, GSI-P-5-78, Darmstadt, 1978.

25. A. Sandoval, J. Harris, R. Stock, L. Schroeder, G. Geaga, et al., to be published.
26. A. Sandoval, private communication.
27. H. H. Gutbrod, W. G. Meyer, A. M. Poskanzer, A. Sandoval, R. Stock, J. Gosset, Ch. King, G. King, Ch. Lukner, N. Van Sen, G. D. Westfall, and K. L. Wolf, unpublished.
28. W. G. Meyer, H. H. Gutbrod, Ch. Lukner, and A. Sandoval, preprint Lawrence Berkeley Laboratory report LBL-9151, to be published in Phys. Rev. C, July 1980.
29. K. K. Gudima, V. D. Toneev, JINR-Dubna P2-10769 (1977) and P2-10431 (1977).
30. R. K. Smith and M. Danos, Fall Creek Falls Conference Proceedings (ORNL CONF-770602, 1977), p. 363.
31. H. Stocker, J. A. Maruhn, and W. Greiner, Z. Physik A243 173-179 (1979).
32. R. Stock, H. H. Gutbrod, W. G. Meyer, A. M. Poskanzer, A. Sandoval, J. Gosset, Ch. King, G. King, Ch. Lukner, N. Van Sen, G. D. Westfall, K. L. Wolf, Phys. Rev. Lett. 44, 1243 (1980).
33. R. Nix, private communication.
34. H. H. Gutbrod, Proceedings of the 4th Summerstudy of Relativistic Nuclear Collisions, July 1978, LBL-7766, p. 1.
35. H. Stöcker and B. Müller, GSI preprint, January 1980.
36. K. K. Gudima and K. D. Toneev, JINR-E2-12624 DUBNA.
37. V. Ruck, M. Gyulassi, and W. Greiner, Z. Physik A277, 391 (1976).
38. G. G. Bunatjan, Yad, Fiz. 29, 258 (1979).

FIGURE CAPTIONS

Fig. 1. The equation of state of nuclear matter as spectulated in various theories. The only quantity known is the state of the normal nuclear density and the approximate curvature through it.

Fig. 2. The fireball model represents the clean-cut separation of nucleons into spectators and participants. It assumes total thermalization.

Fig. 3. Double differential cross-sections of protons from Ne on U at four different incident energies. Lines represent a fire streak calculation for emitted protons.

Fig. 4. Double differential cross section of protons from 393 MeV/u ^{20}Ne interactions with Al, Ag, Au and U. Lines represent the firestreak calculation for emitted protons.

Fig. 5. Precentage of protons observed in emitted clusters of α, t, ^{3}He and ^{4}He vs emitted protons.

Fig. 6. Neutron to proton ratio corrected for cluster emission observed and calculated in a cascade model by Stevenson[11]).

Fig. 7. Summed charge spectra from reactions of 393 MeV/u ^{20}Ne on U compared with intranuclear cascade calculations of Fraenkel and Yariv[15]) and with hydrodynamical calculations from R. Nix et al.[16]).

Fig. 8. Double differential cross section of Boron emitted from the reaction of 393 MeV/u ^{20}Ne on U. The straight line represents a fit assuming a moving emitting system with a temperature of 27 MeV.

Fig. 9. Contours of constant invariant cross section for positive pions produced in reactions of 1.05 GeV/u ^{40}Ar with ^{40}Ca or in the reaction of 370 MeV p on hydrogen.

Fig. 10. Calculations of π^+ production assuming a fireball-like long-lived pion source and Coulomb effects influencing the pion-emission.

Fig. 11. Experimental layout of the scattering-chamber and the various detector systems.

Fig. 12. Charged particle multiplicity distribution associated with the observation of a proton from 42 GeV Ne and 42 GeV Ar on U.

Fig. 13. Average multiplicity of charged particles associated with a proton, deuteron or triton emitted from reactions on a U target.

Fig. 14. The average multiplicity depends on the total kinetic energy for small projectiles and large targets.

Fig. 15. Slow fragment-fast particle correlation showing an enhancement of coincidences at 180^{o} in ϕ. This suggests the establishment of a reaction plane by the target, the heavy fragment observed in the telescope and by the bulk of the fast particles associated with the slow heavy fragment.

Fig. 16. Density contours as calculated in a hydrodynamical model. The experimentally observed bounce-off is shown to be dependent of the impact parameter.

Fig. 17. Fragment spectra of Carbon to Na from 1.05 GeV/u ^{4}He on Au with Coulomb peak shifting with increasing Z.

Fig. 18. Density contours as calculated in a hydrodynamical model. Note the bowl shape of the system strongly oriented with respect to the beam direction at a late state resulting in quite different Coulomb effects for different polar angles of emission.

Fig. 19. Contours of invariant cross section for 1.8 GeV/u ^{40}Ar or KCl in the plane of negative-pion multiplicity vs total charged particle multiplicity. The straight line indicates the complete disintegration of both target and projectile nuclei.

Fig. 20. Double differential cross sections of protons from events selected for low or high associated charged particle multiplicity.

Fig. 21. Multiplicity selections for various targets.

Fig. 22. Contours of constant invariant cross section in a $p_{\perp}$ vs y plane for high or low multiplicity protons from 20 Ne on U at 393 MeV/u.

Fig. 23. Contours of constant invariant cross section in a $p_{\perp}$ vs y plane for high or low multiplicity protons from 1.05 Gev/u ^{40}Ar on ^{40}Ca.

Fig. 24. Angular distribution of fragment-emission at fixed fragment momenta for 400 MeV/u ^{20}Ne on U.

Fig. 25. Angular distribution of fragment emission at fixed fragment momenta for 2.1 GeV/u ^{20}Ne on U.

Fig. 26. Low energy protons selected for high or low multiplicity from 42 GeV Ne and Ar on U and from 393 MeV/u Ne on U.

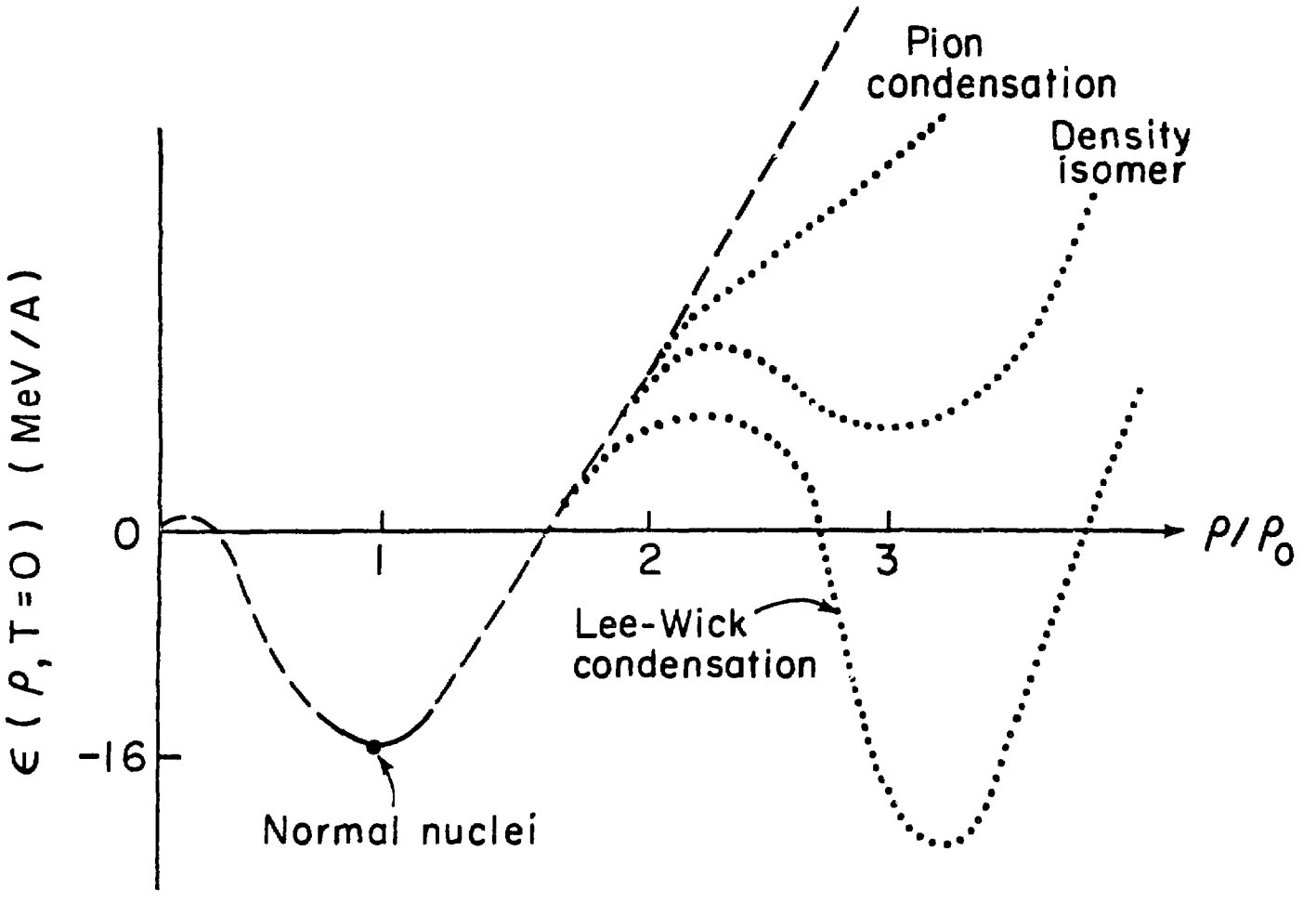
Pion
condensation
Density
isomer
$\epsilon(\rho, T=0)$ (MeV/A)
0
-16
1
2
3
ρ/ρ_0
Lee-Wick
condensation
Normal nuclei
XBL767-3223

Fig. 1

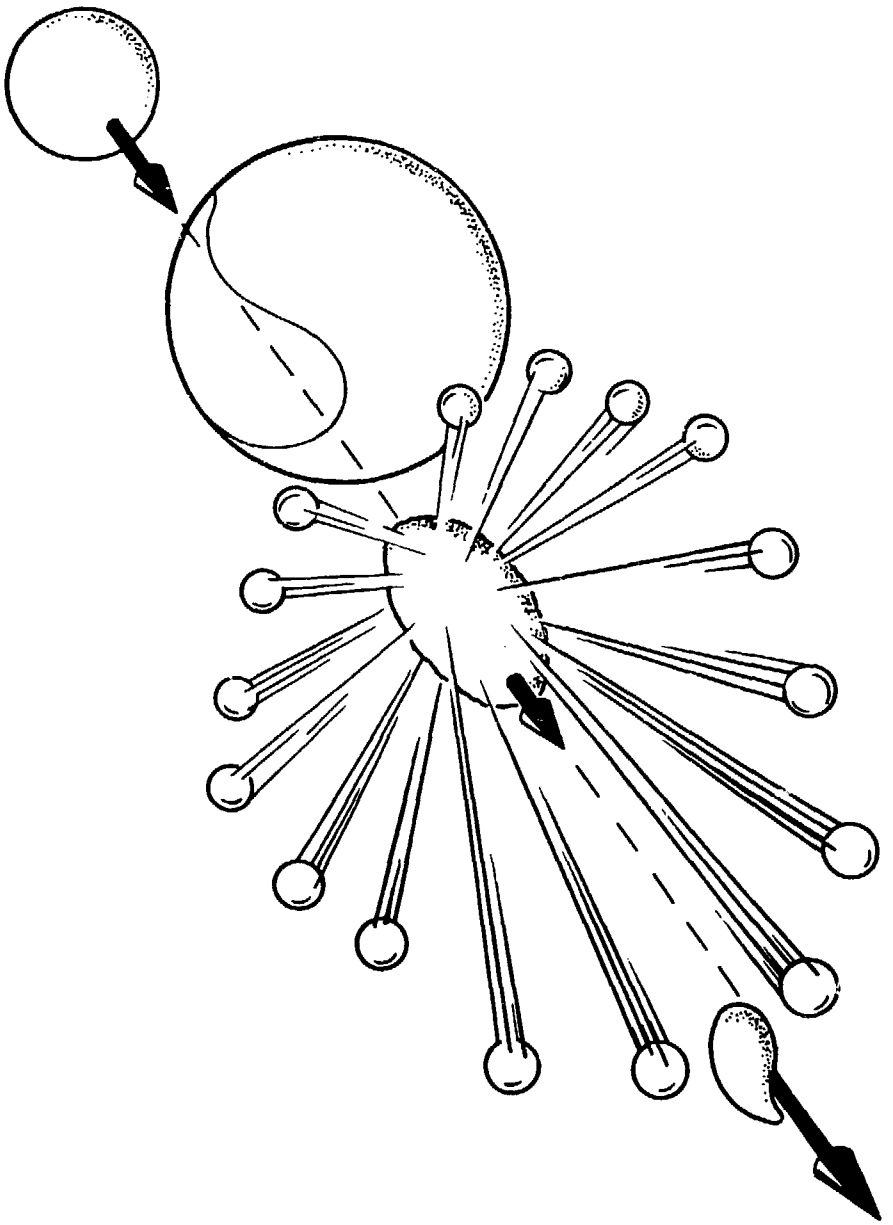

XBL 7610-4267

Fig. 2

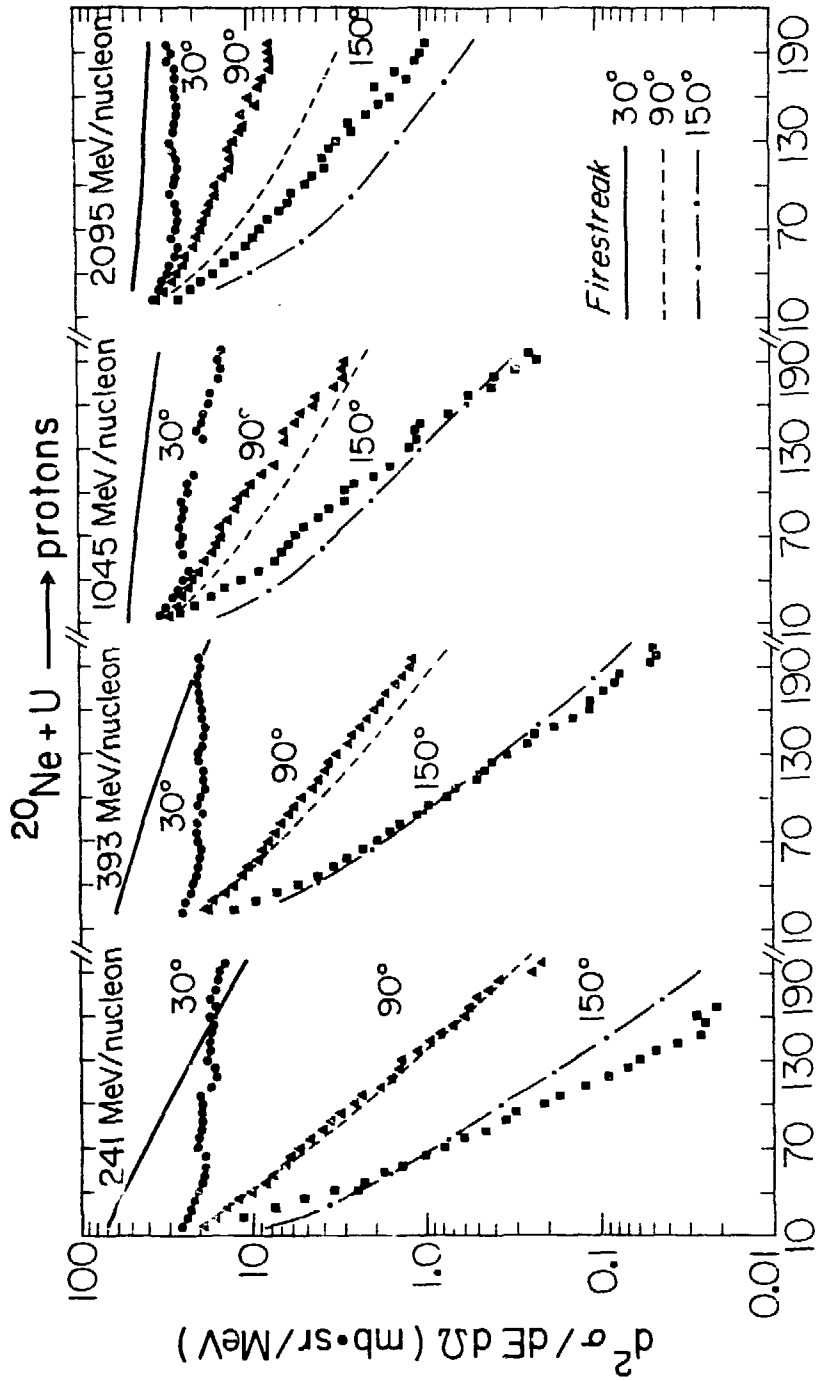

XBL 7912-13547

Fig. 3

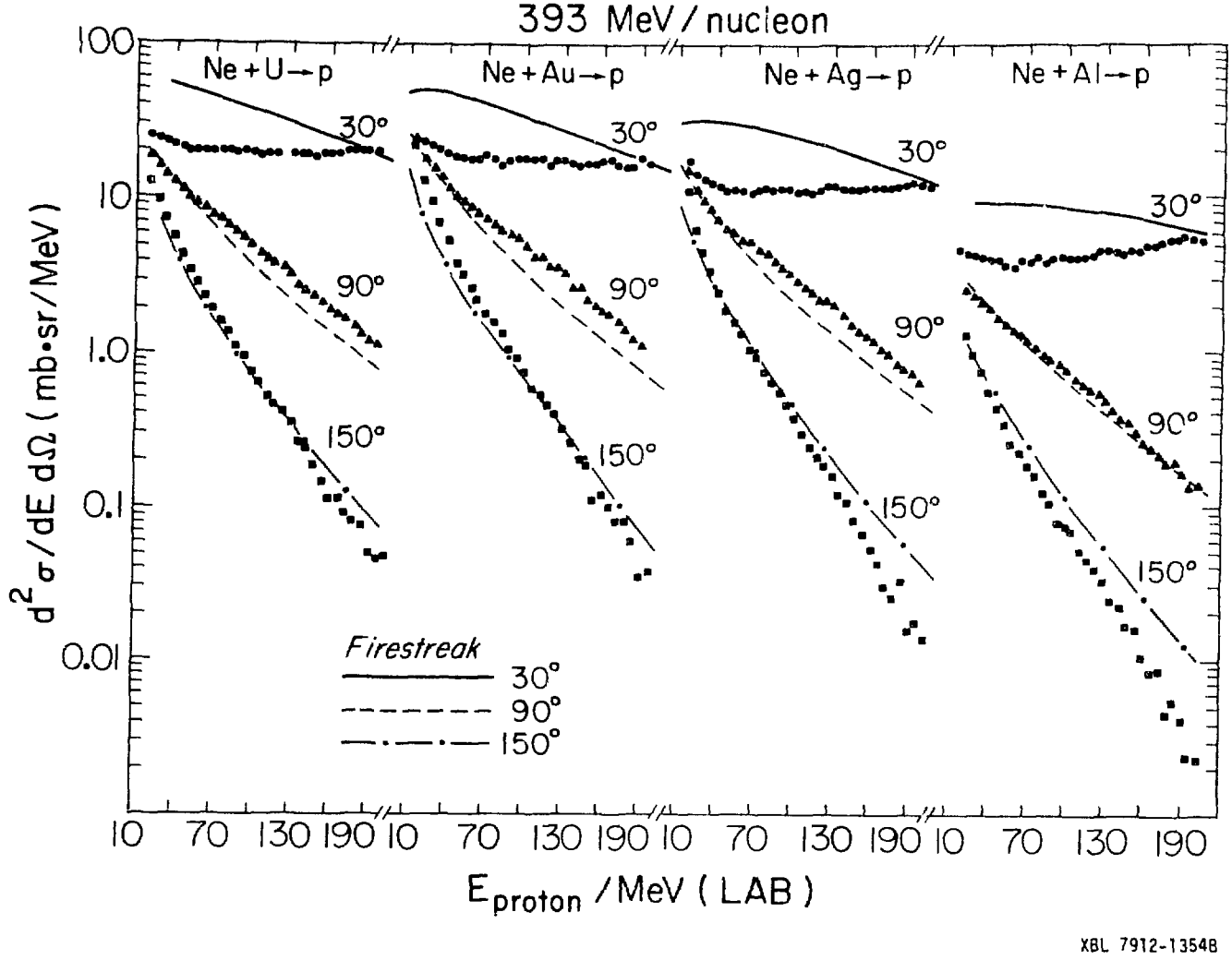

XBL 7912-13548

Fig. 4

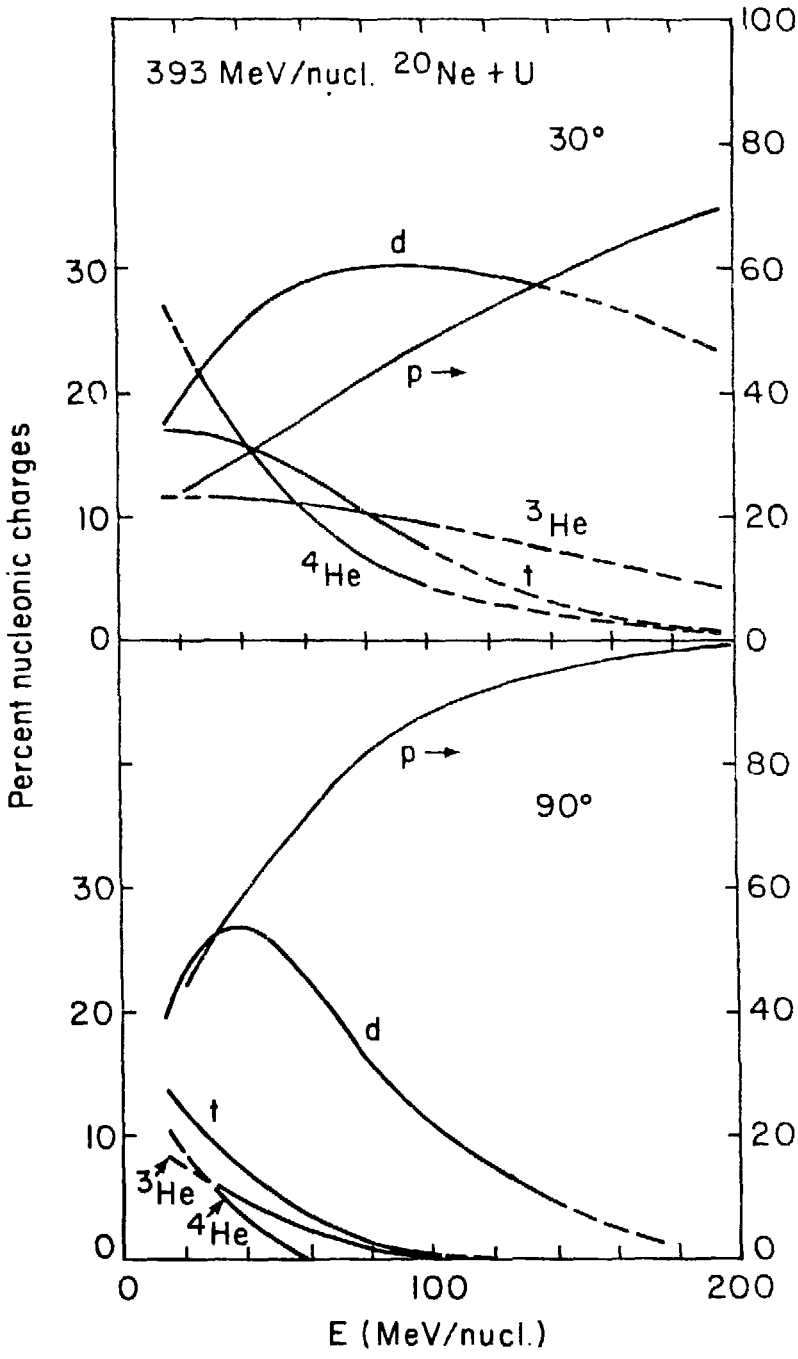
393 MeV/nucl. 20Ne + U
30°
90°
d
p
3He
4He
t
Percent nucleonic charges
E (MeV/nucl.)
0
10
20
30
40
60
80
100
200
XBL 797-2268

Fig. 5

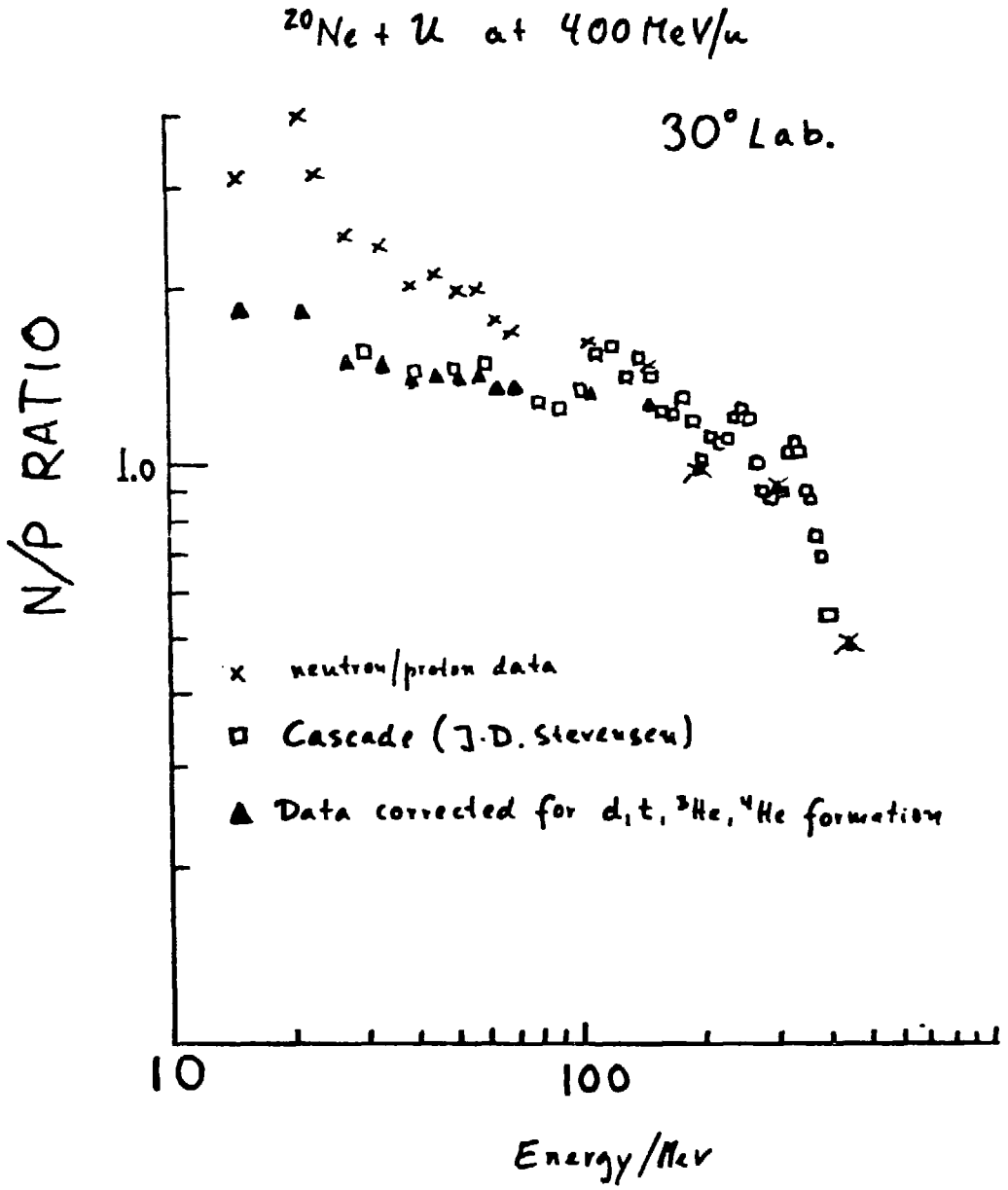
$^{20}Ne + U$ at 400 MeV/u
30° Lab.
N/P RATIO
1.0
neutron/proton data
Cascade (J.D. Stevenson)
Data corrected for d, t, ^3He, ^4He formation
10
100
Energy/Mev

Fig. 6

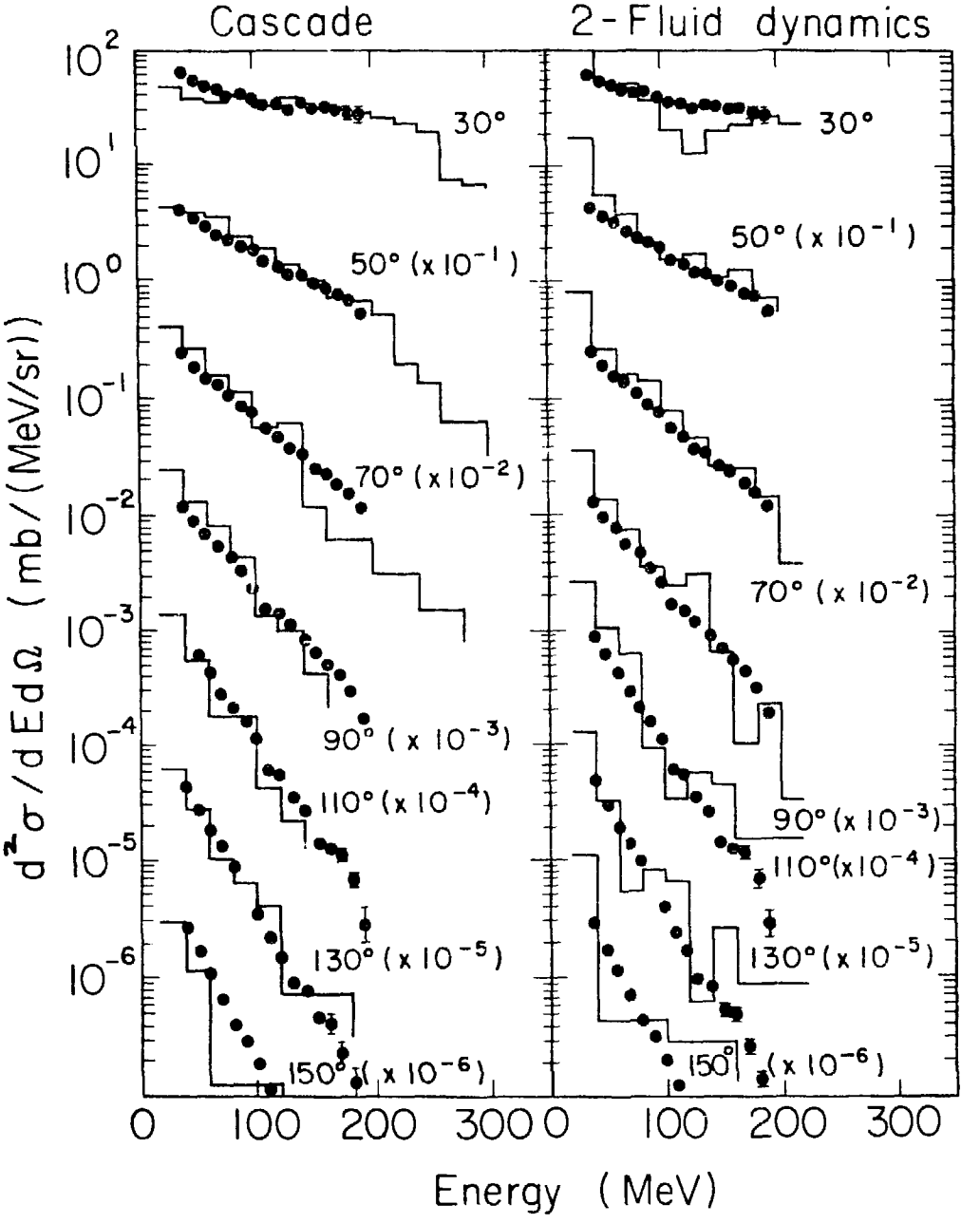
Cascade
2-Fluid dynamics
30°
50° (x 10⁻¹)
70° (x 10⁻²)
90° (x 10⁻³)
110° (x 10⁻⁴)
130° (x 10⁻⁵)
150° (x 10⁻⁶)
d²σ/dEdΩ (mb/(MeV/sr))
Energy (MeV)
0
100
200
300
XBL787-1372

Fig. 7

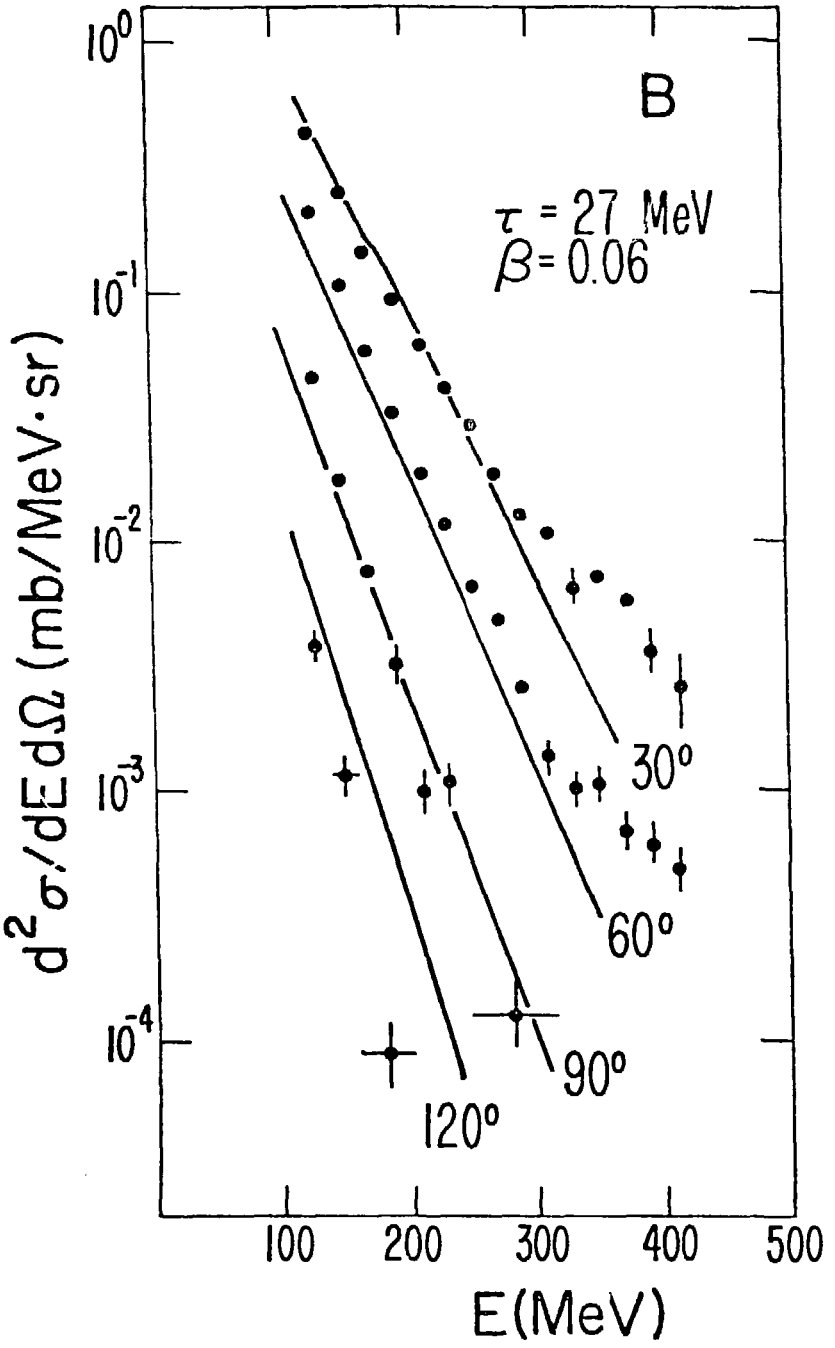

XBL 774-891

Fig. 8

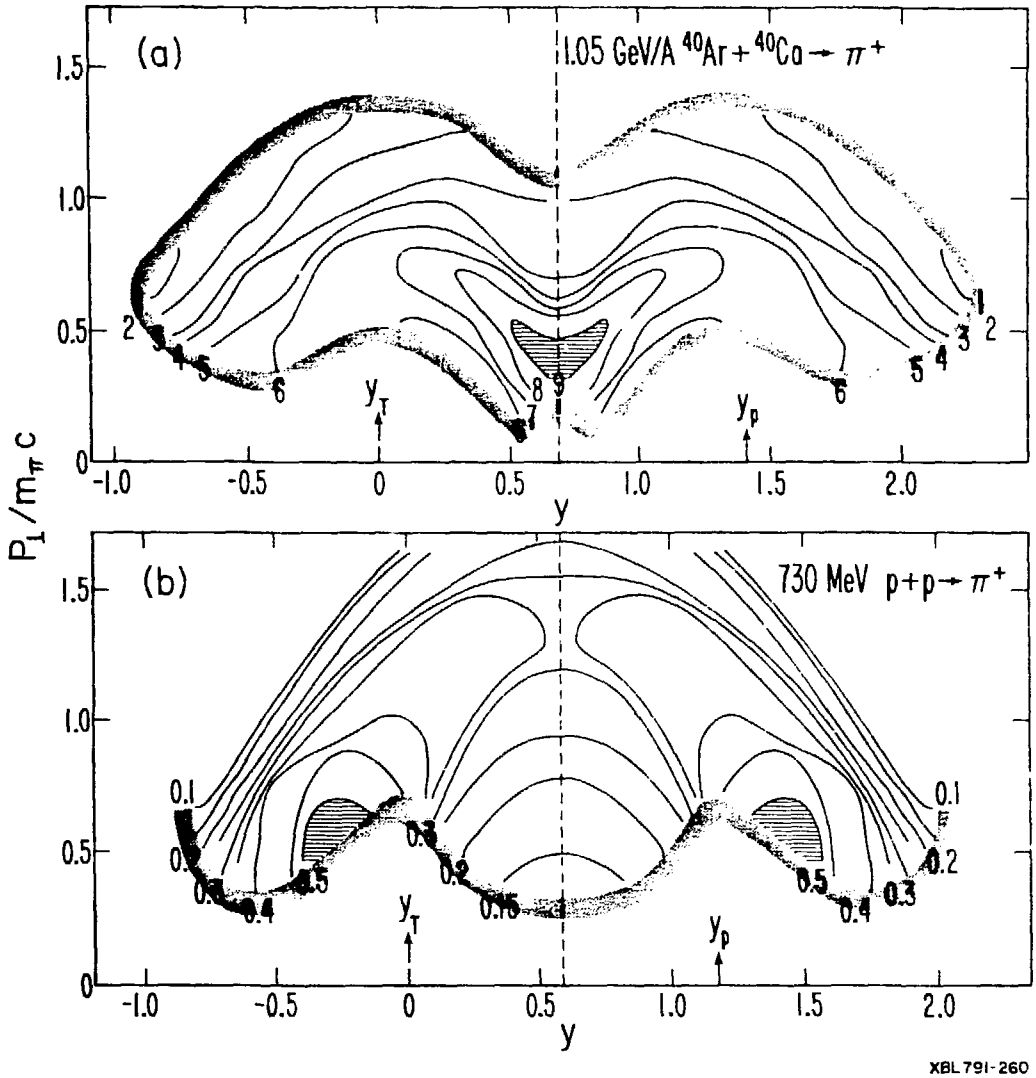
(a)
1.05 GeV/A $^{40}Ar + ^{40}Ca \rightarrow \pi^+$
(b)
730 MeV $p+p \rightarrow \pi^+$
$P_1/m_\pi c$
y
y_T
y_p
XBL791-260

Fig. 9

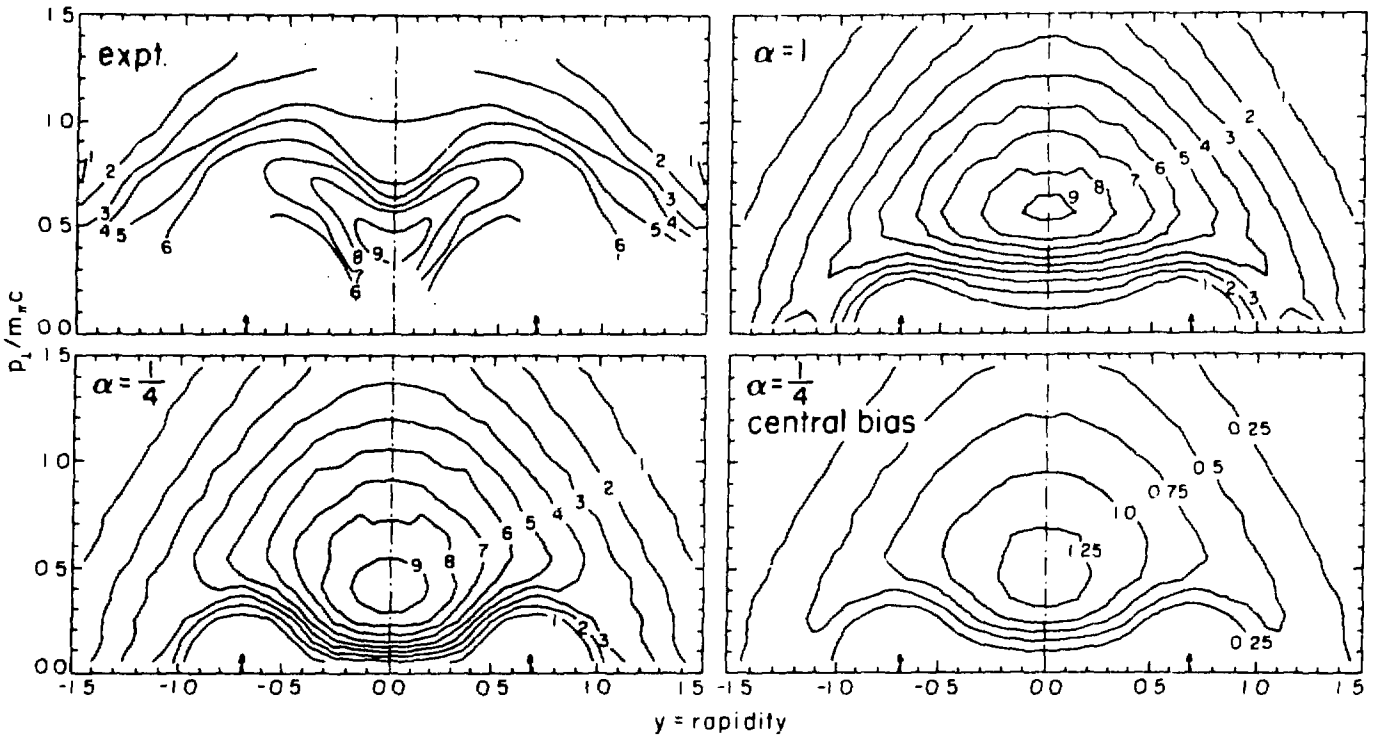

Fig. 10

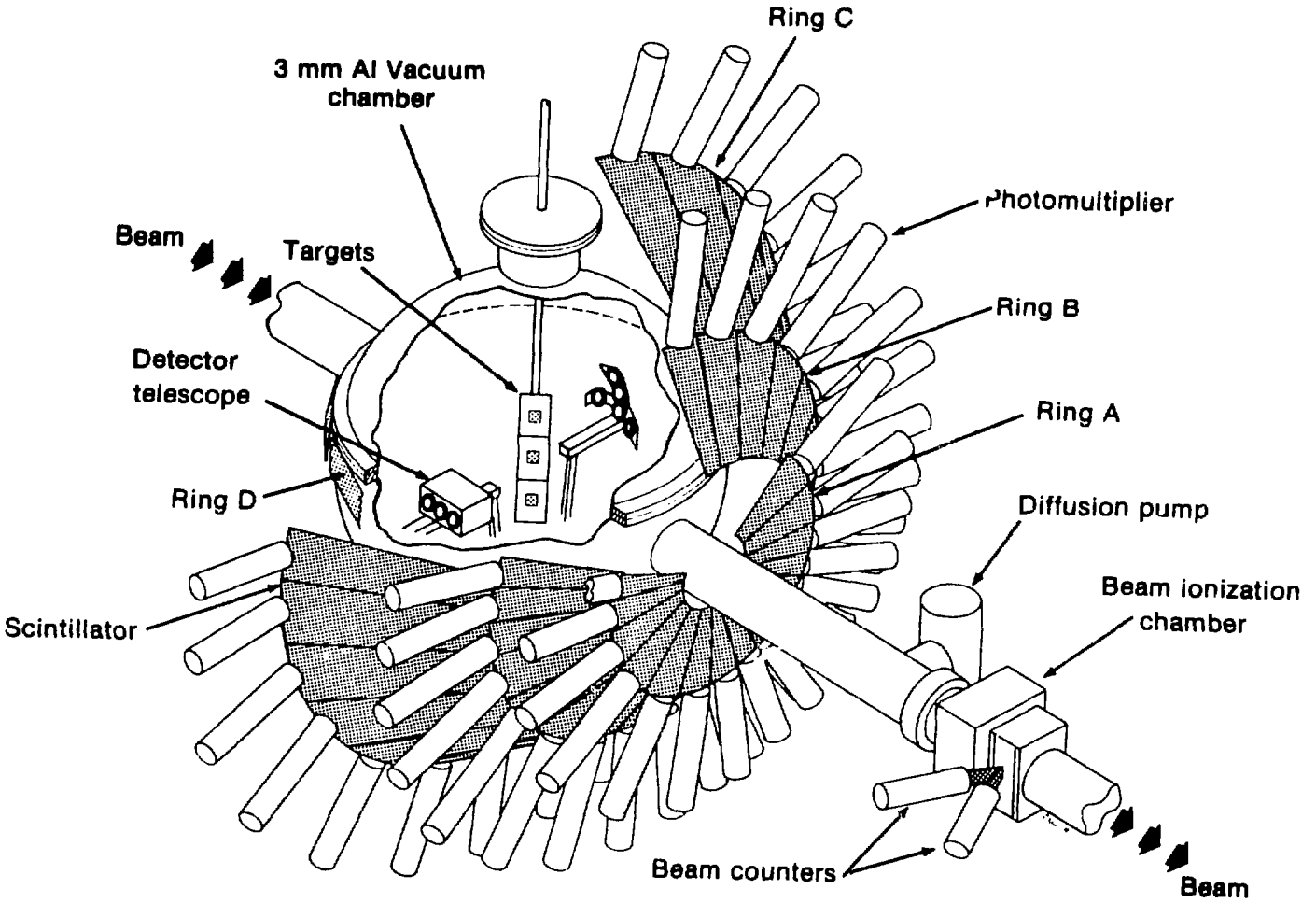

XBL 782-7229 D

Fig. 11

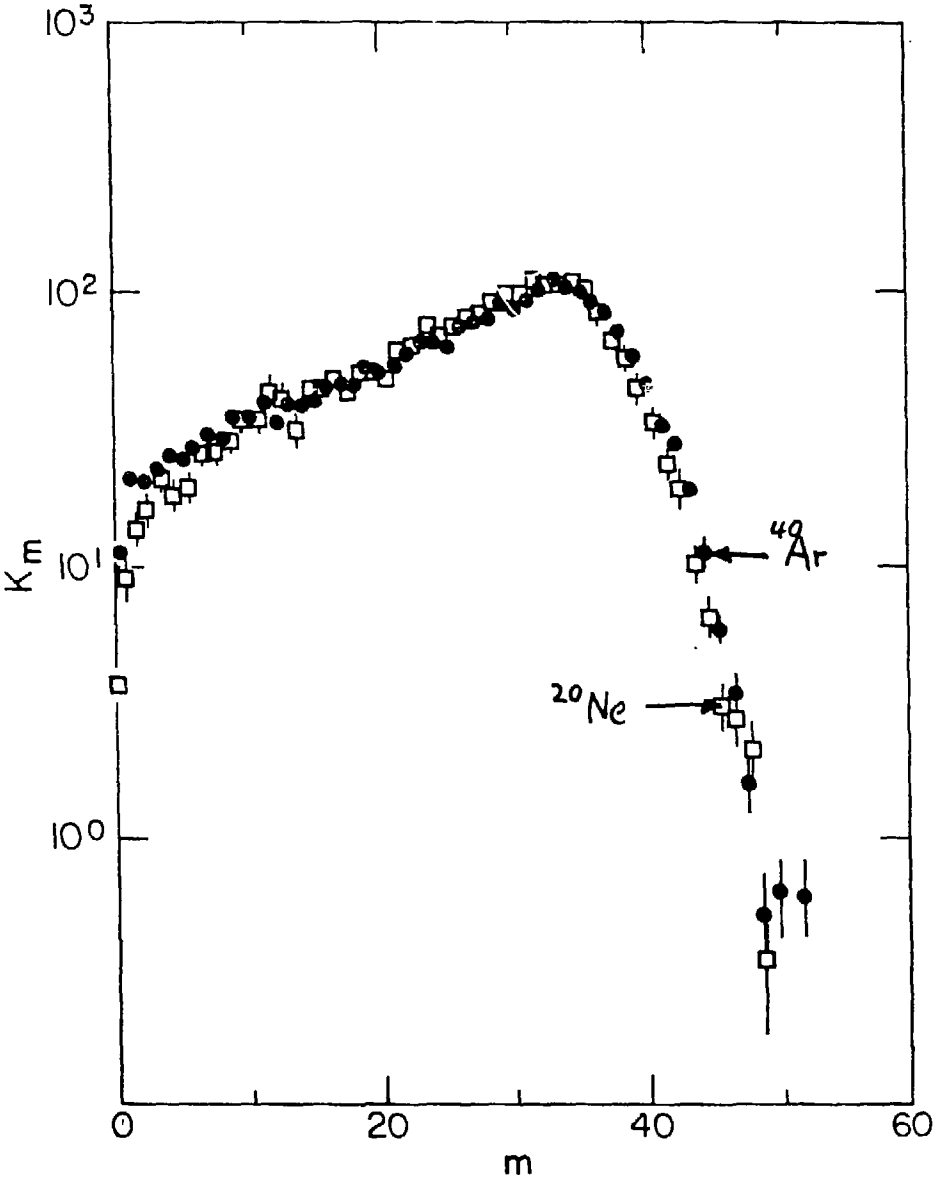

XBL 797-2052

Fig. 12

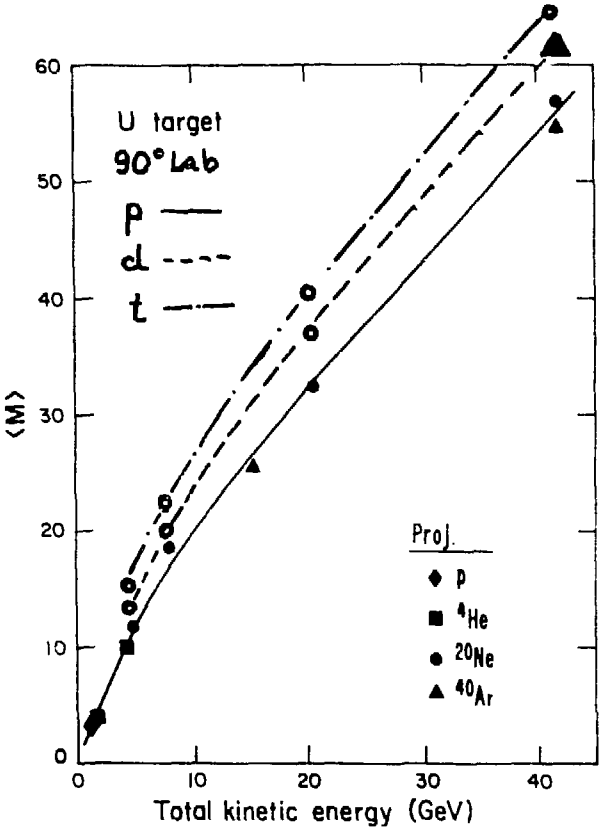

XBL 797 - 2054

Fig. 13

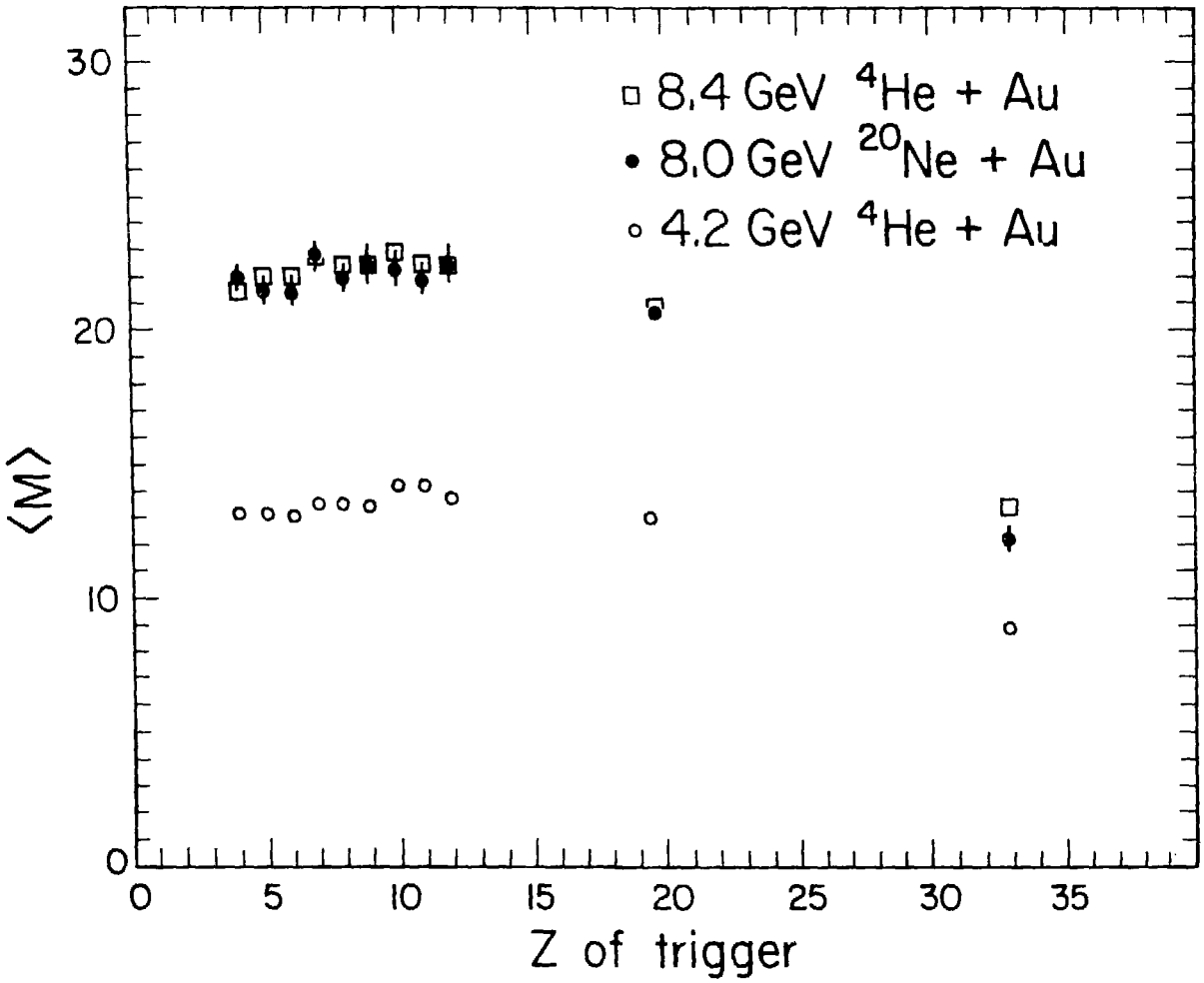

XBL 797-2135

Fig. 14

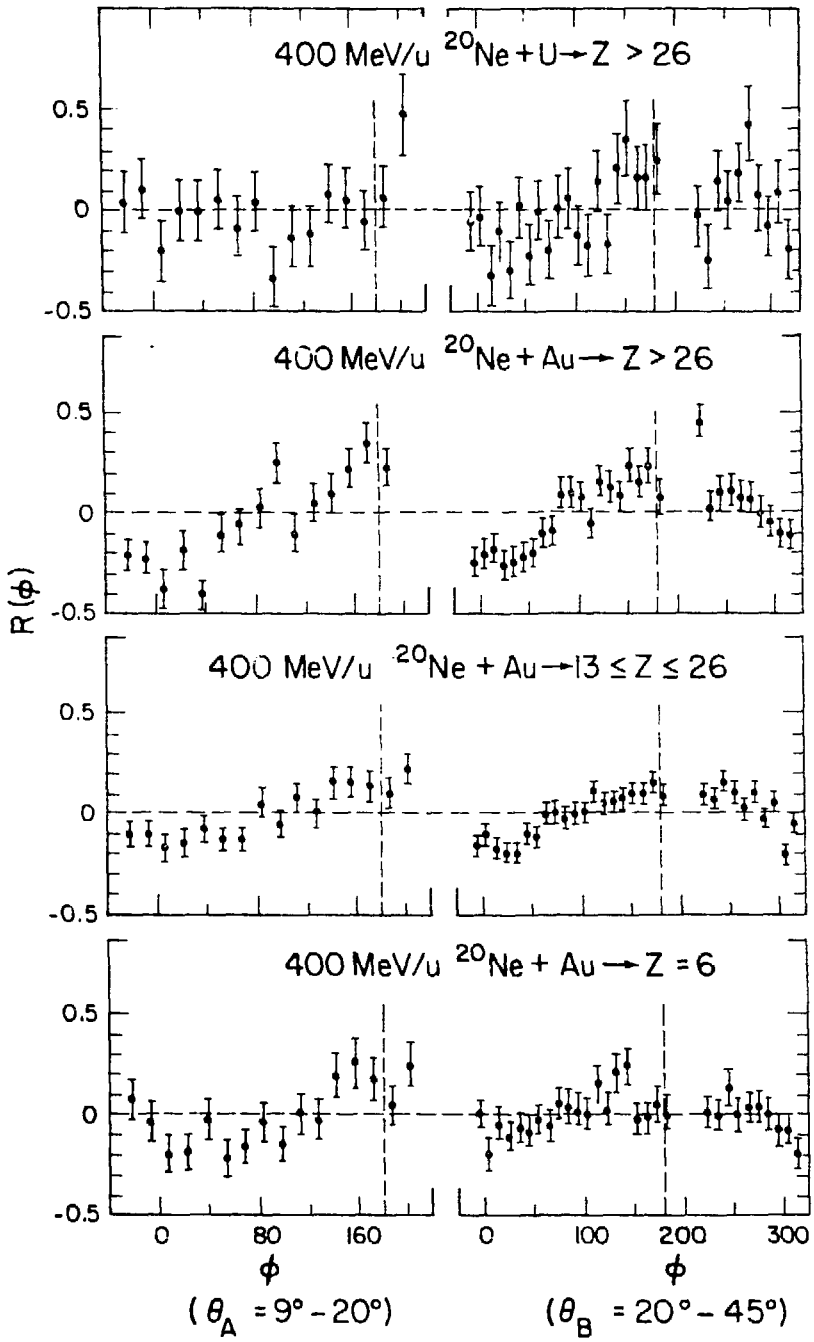
400 MeV/u ^{20}Ne + U → Z > 26
400 MeV/u ^{20}Ne + Au → Z > 26
400 MeV/u ^{20}Ne + Au → 13 ≤ Z ≤ 26
400 MeV/u ^{20}Ne + Au → Z = 6
R(φ)
0.5
0
-0.5
0
80
160
100
200
300
φ
φ
(θ_A = 9° - 20°)
(θ_B = 20° - 45°)
XBL 797-2210

Fig. 15

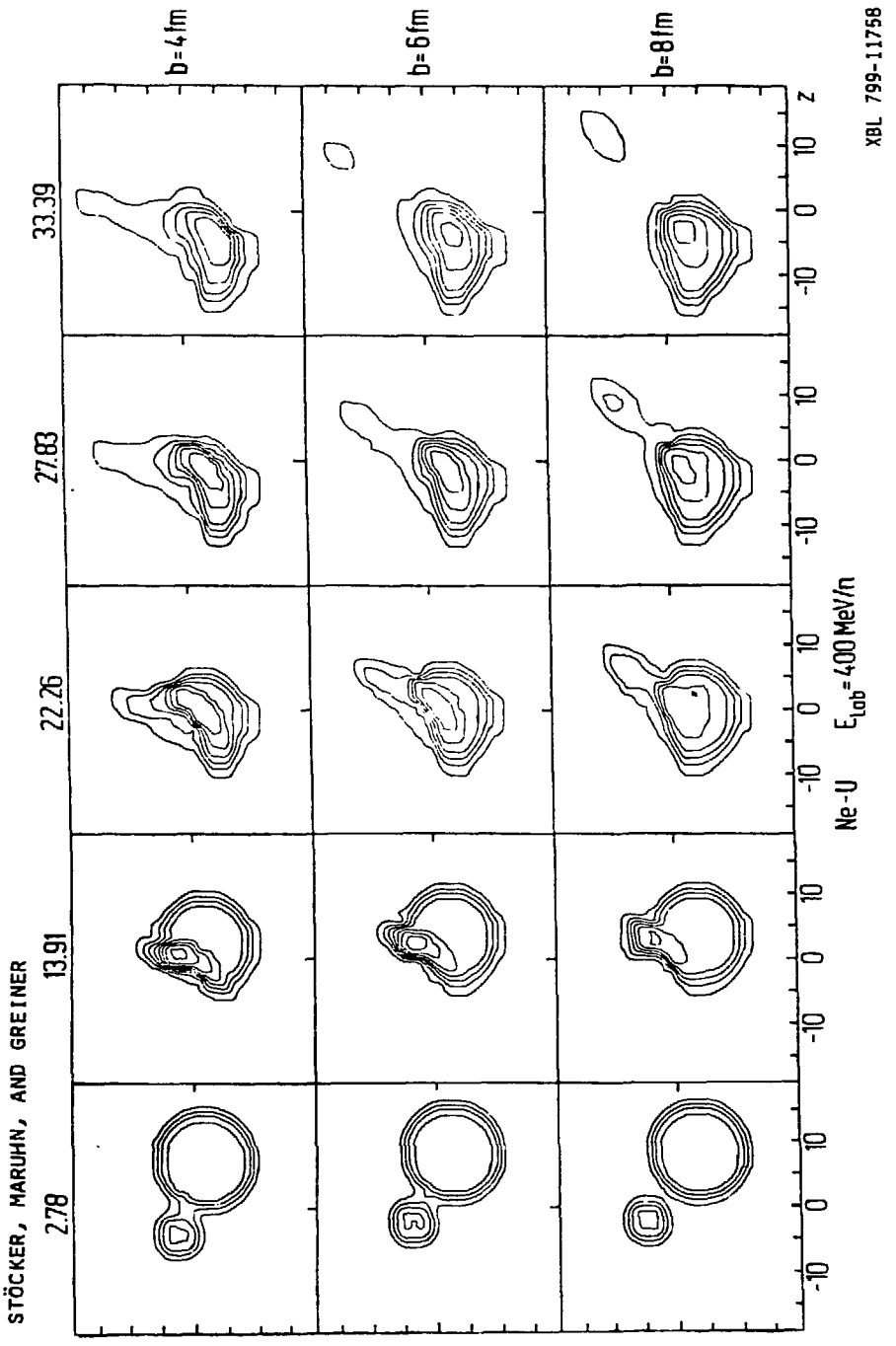
STÖCKER, MARUHN, AND GREINER
2.78
13.91
22.26
27.83
33.39
b=4fm
b=6fm
b=8fm
-10
0
10
z
Ne-U E_{Lab}=400 MeV/n
XBL 799-11758

Fig. 16

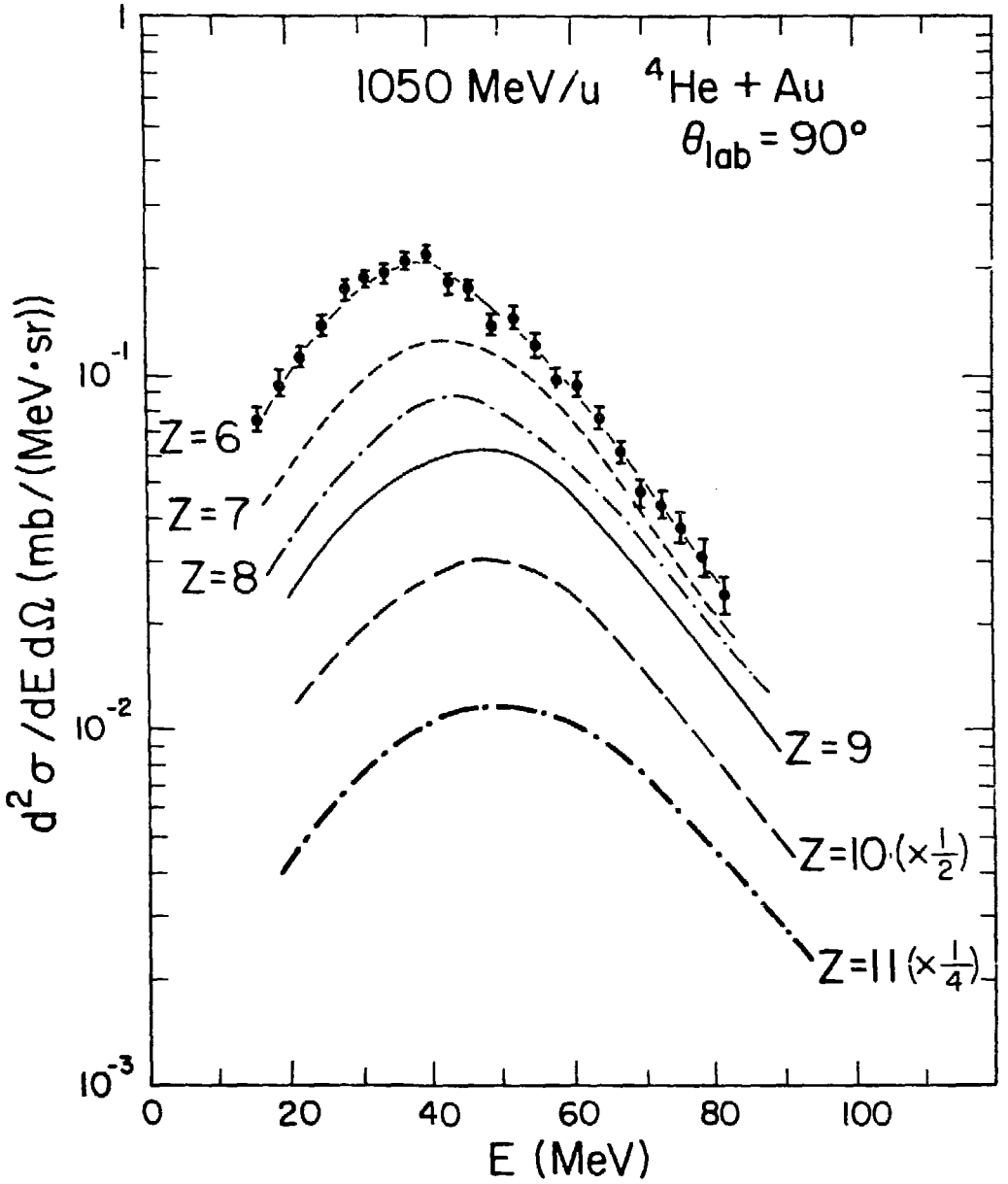

XBL 797-2209

Fig. 17

STÖCKER, MARUHN, AND GREINER

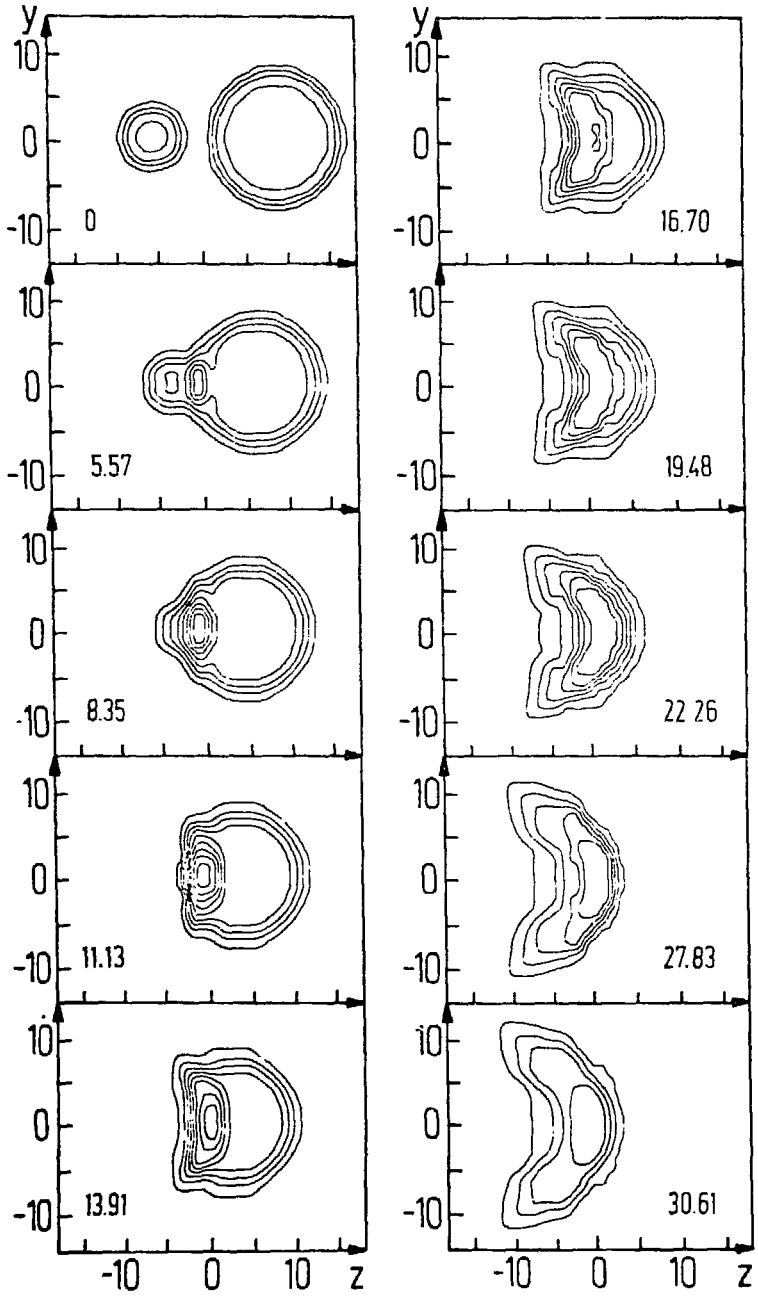

XBL 799-11757

Fig. 18

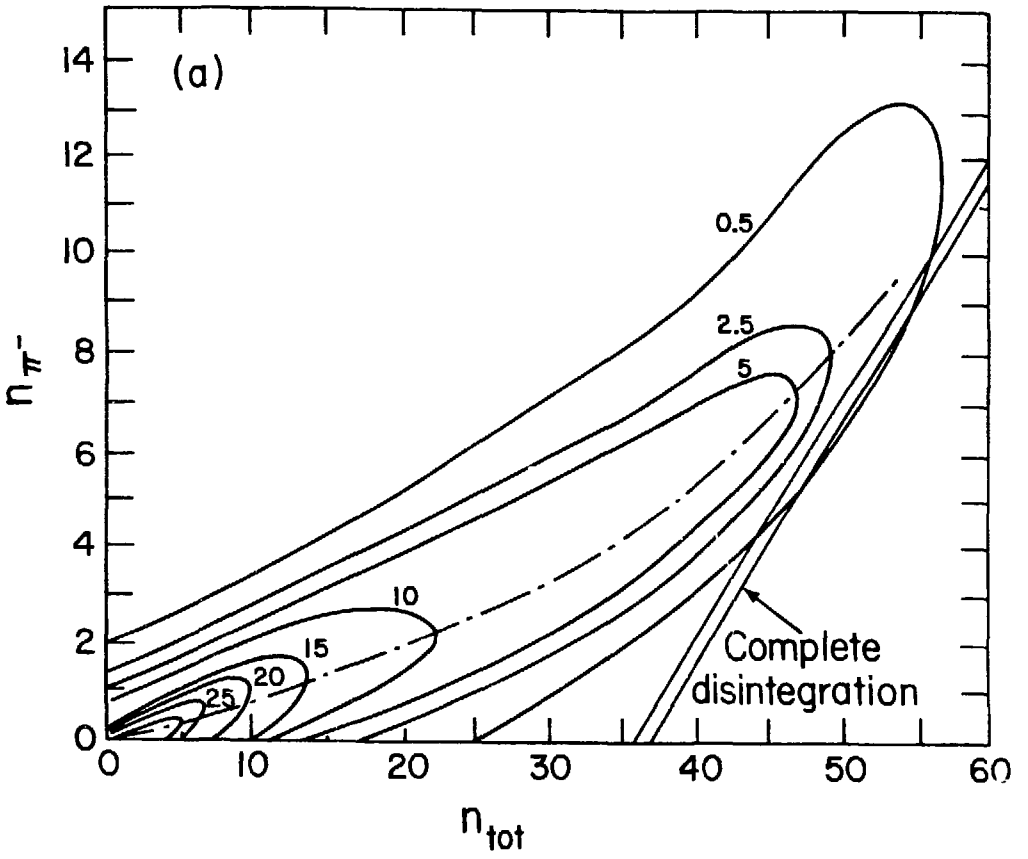

XBL804-702

Fig. 19

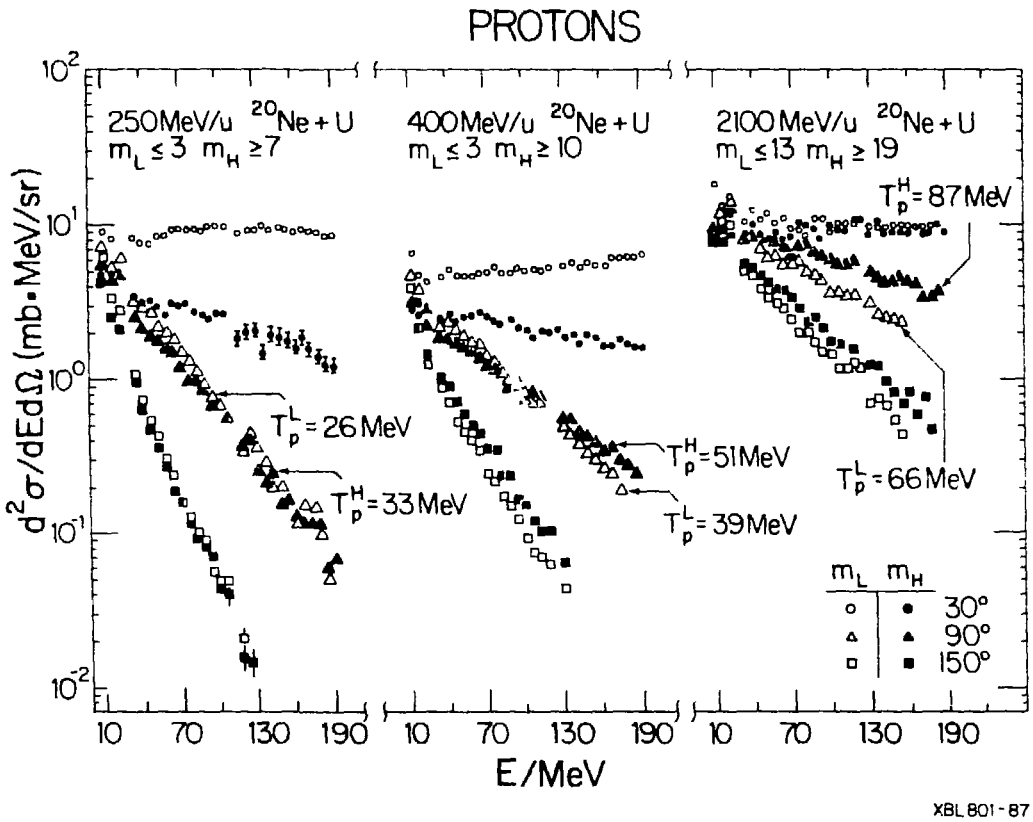
PROTONS
250MeV/u ^{20}Ne + U
$m_L \leq 3$ $m_H \geq 7$
400MeV/u ^{20}Ne + U
$m_L \leq 3$ $m_H \geq 10$
2100MeV/u ^{20}Ne + U
$m_L \leq 13$ $m_H \geq 19$
T_p^H = 87MeV
T_p^L = 26MeV
T_p^H = 33MeV
T_p^H = 51MeV
T_p^L = 39MeV
T_p^L = 66MeV
m_L m_H
30°
90°
150°
$d^2\sigma/dEd\Omega$ (mb•MeV/sr)
E/MeV
XBL801-87

Fig. 20

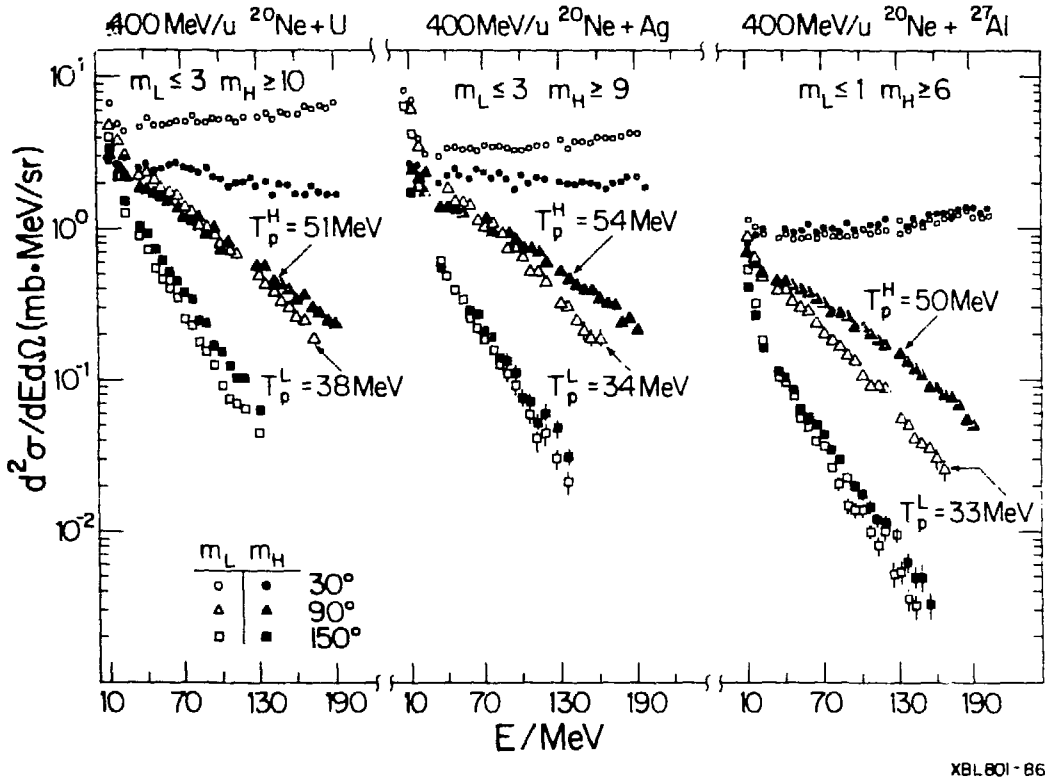
400 MeV/u ^{20}Ne + U
400MeV/u ^{20}Ne + Ag
400MeV/u ^{20}Ne + ^{27}Al
$m_L \leq 3$ $m_H \geq 10$
$m_L \leq 3$ $m_H \geq 9$
$m_L \leq 1$ $m_H \geq 6$
T_p^H = 51MeV
T_p^L = 38MeV
T_p^H = 54MeV
T_p^L = 34MeV
T_p^H = 50MeV
T_p^L = 33MeV
m_L m_H
30°
90°
150°
$d^2\sigma/dEd\Omega$ (mb·MeV/sr)
E/MeV
XBL801-86

Fig. 21

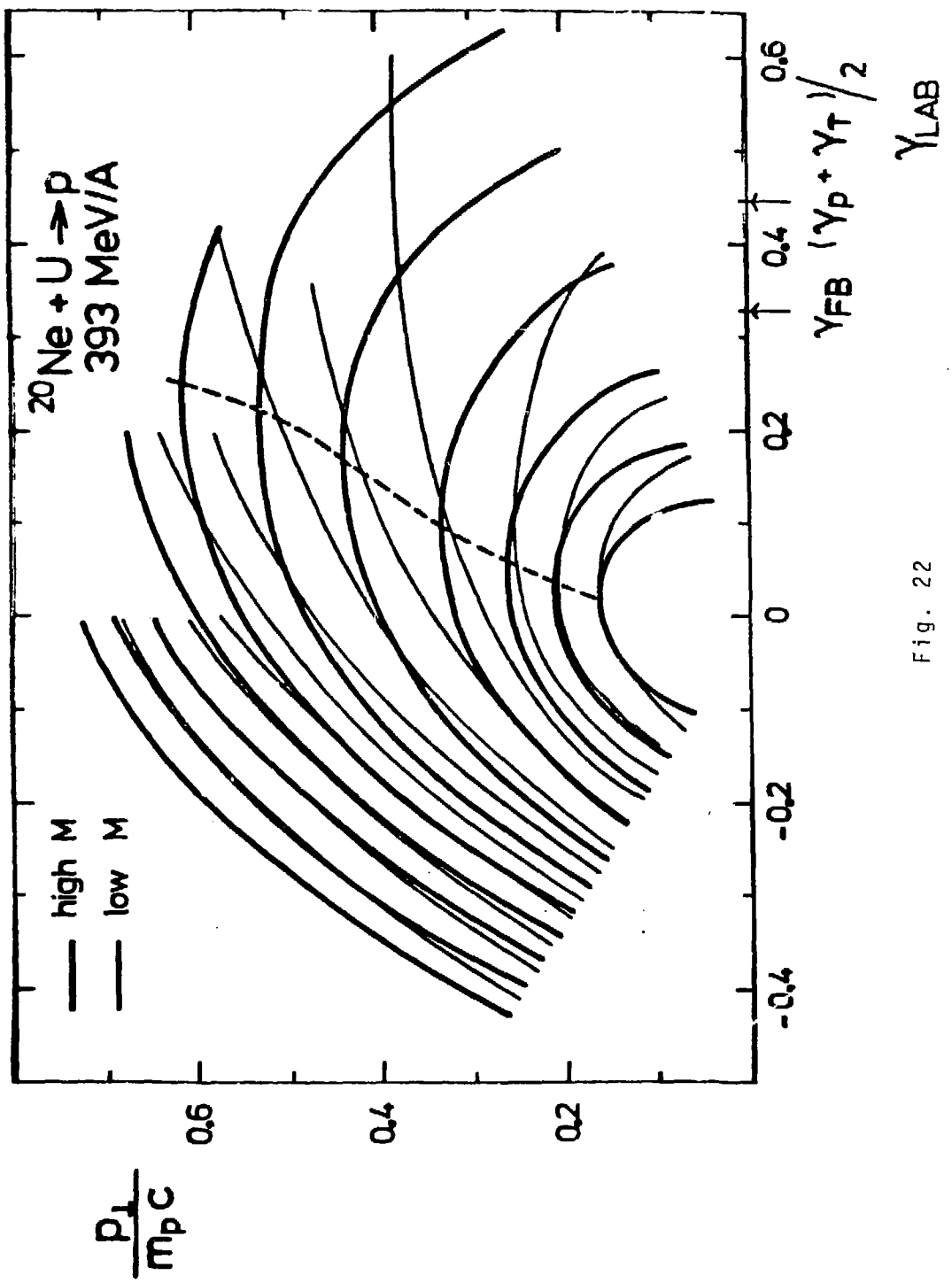
$\frac{p_\perp}{m_p c}$
0.6
0.4
0.2
high M
low M
$^{20}Ne + U \rightarrow p$
393 MeV/A
-0.4
-0.2
0
0.2
0.4
0.6
y_{FB} ($y_p + y_T$)/2
y_{LAB}

Fig. 22

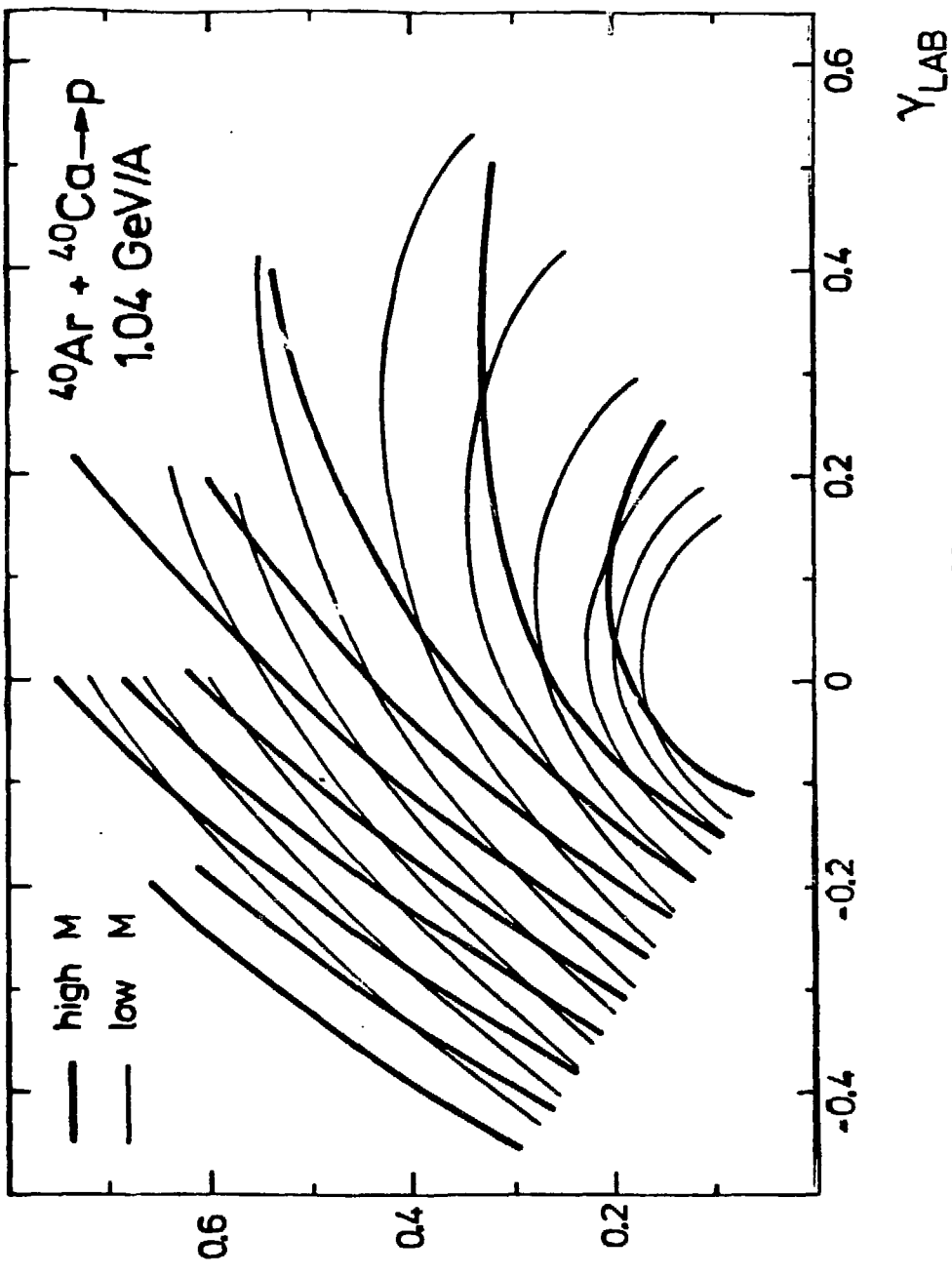
$\frac{P_\perp}{m_p c}$
0.6
0.4
0.2
high M
low M
$^{40}Ar + ^{40}Ca \rightarrow p$
1.04 GeV/A
-0.4
-0.2
0
0.2
0.4
0.6
Y_{LAB}

Fig. 23

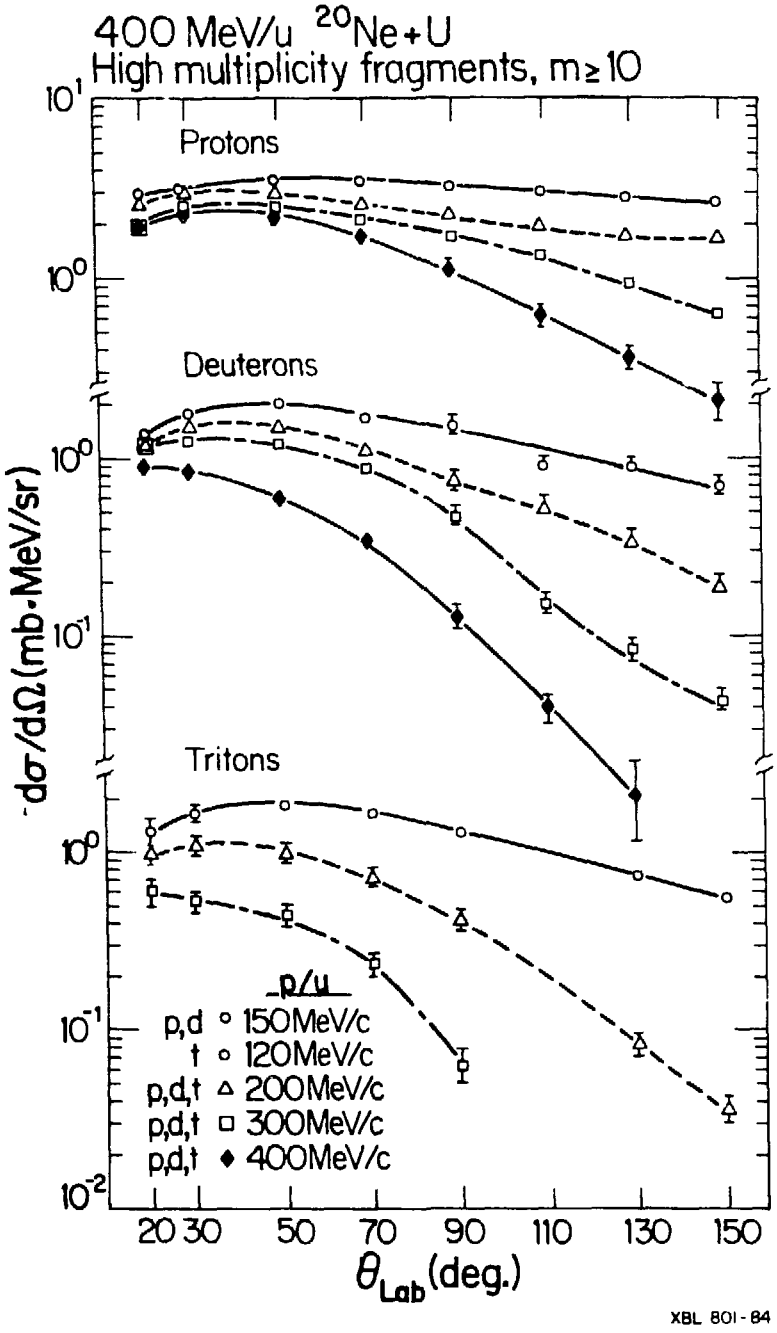
400 MeV/u ^{20}Ne+U
High multiplicity fragments, m≥10
Protons
Deuterons
Tritons
-dσ/dΩ(mb·MeV/sr)
θ$_{Lab}$(deg.)
p/u
p,d ○ 150MeV/c
t ○ 120MeV/c
p,d,t △ 200MeV/c
p,d,t □ 300MeV/c
p,d,t ♦ 400MeV/c
XBL 801-84

Fig. 24

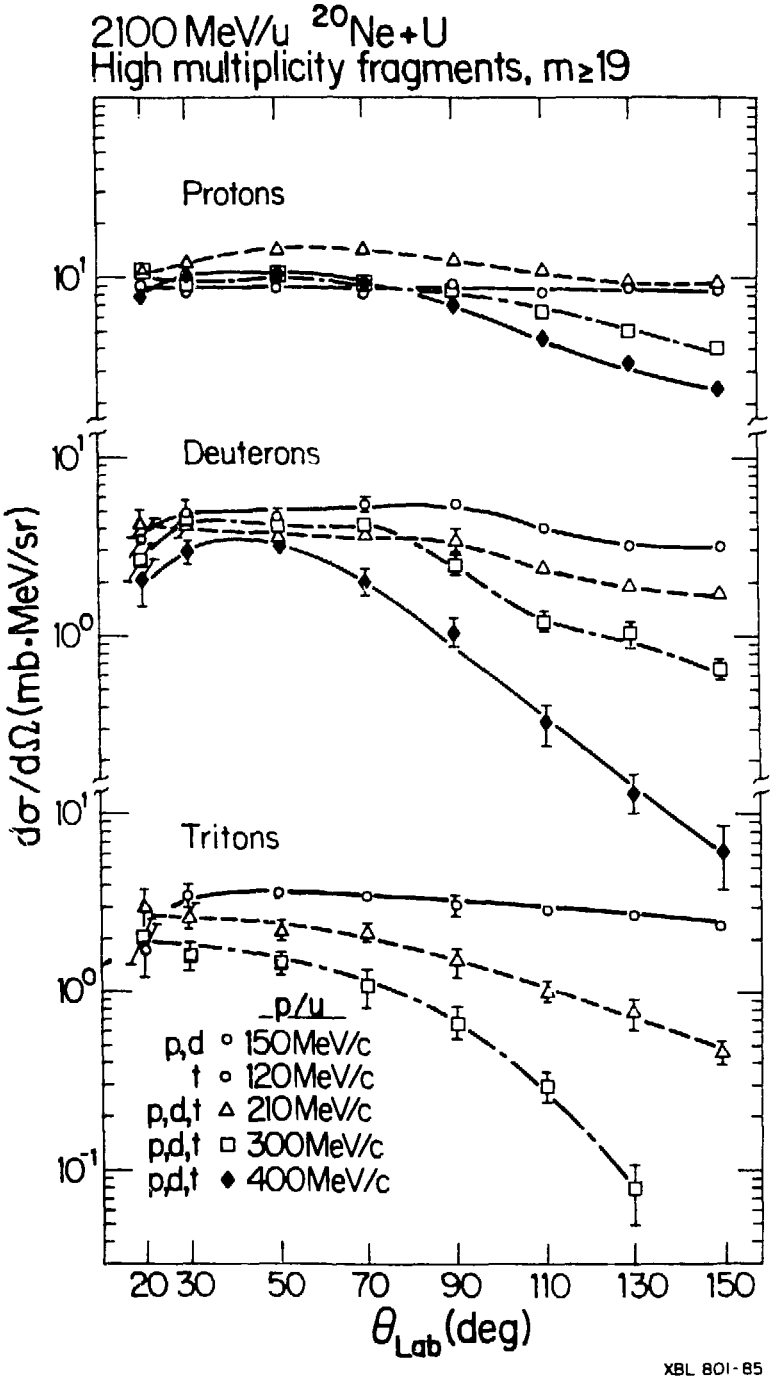
2100 MeV/u ^{20}Ne+U
High multiplicity fragments, m≥19
Protons
Deuterons
Tritons
$d\sigma/d\Omega$(mb·MeV/sr)
p/u
p,d ○ 150MeV/c
t ○ 120MeV/c
p,d,t △ 210MeV/c
p,d,t □ 300MeV/c
p,d,t ◆ 400MeV/c
θ_{Lab}(deg)
XBL 801-85

Fig. 25

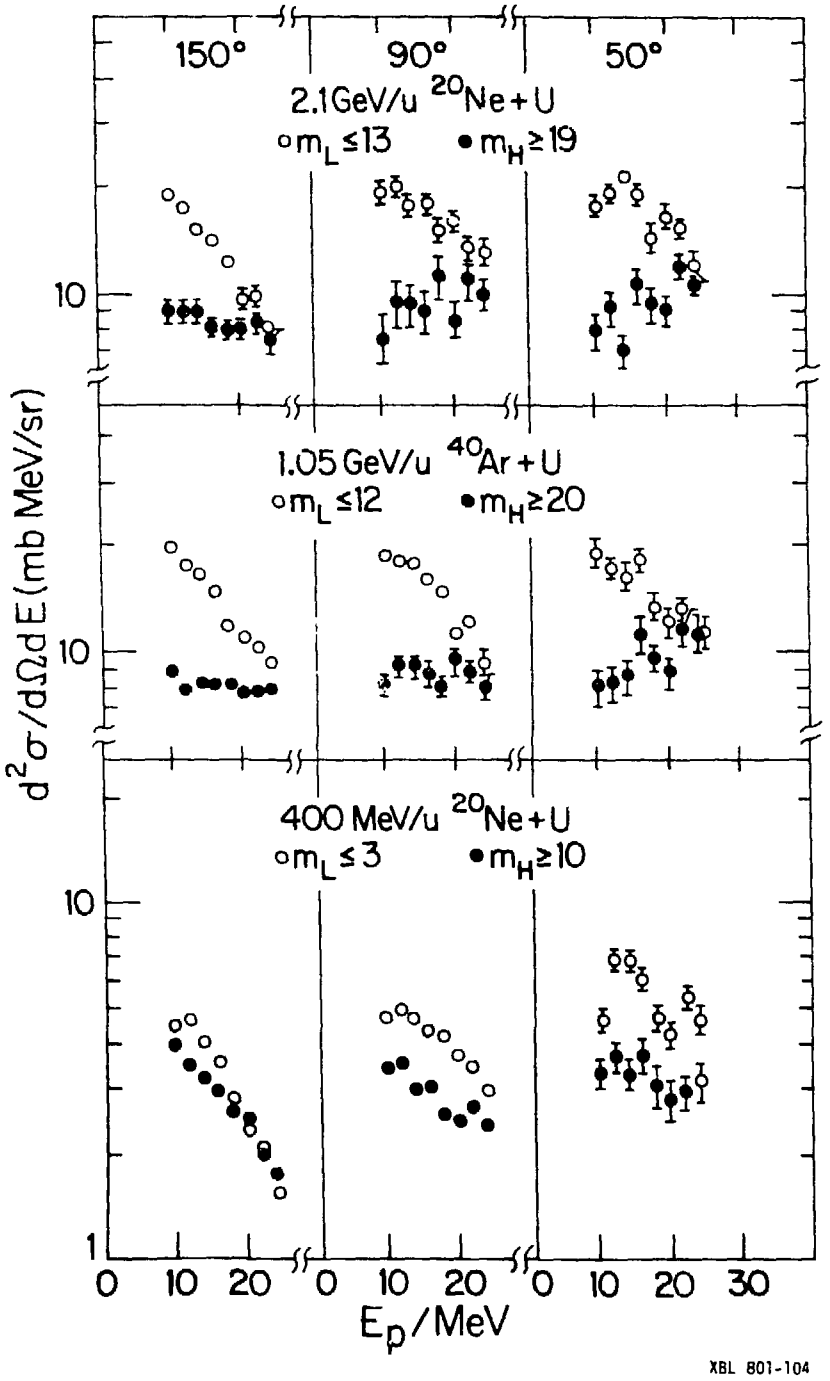
150°
90°
50°
2.1GeV/u ^{20}Ne+U
$m_L \leq 13$
$m_H \geq 19$
1.05 GeV/u ^{40}Ar+U
$m_L \leq 12$
$m_H \geq 20$
400 MeV/u ^{20}Ne+U
$m_L \leq 3$
$m_H \geq 10$
$d^2\sigma/d\Omega dE$ (mb MeV/sr)
E_p/MeV
XBL 801-104

Fig. 26

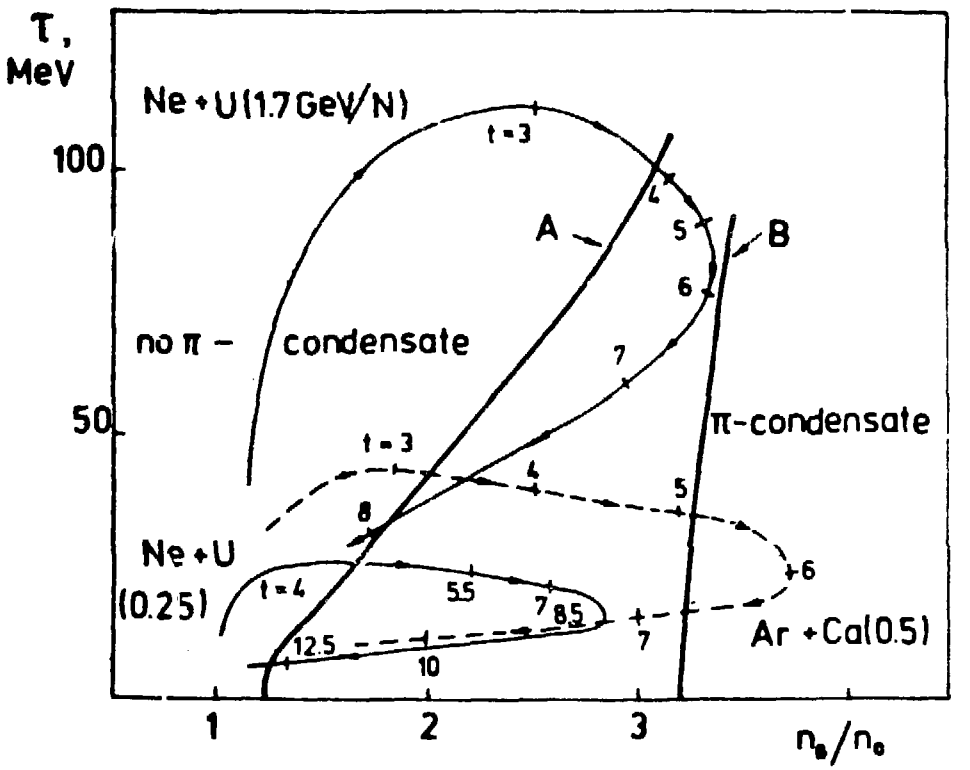

XBL 806-10364

Fig. 27